Journal of Geochemical Exploration

Zirconium and hafnium fractionation and distribution of rare earth elements in neutral - alkaline waters: Case study of Lake Van hydrothermal system, Turkey

--Manuscript Draft--

Manuscript Number:	GEXPLO-D-20-00114R1
Article Type:	Research Paper
Keywords:	Zr/Hf ratio; REE; Alkaline lakes; Turkey
Corresponding Author:	Paolo Censi University of Palermo: Universita degli Studi di Palermo ITALY
First Author:	Ahmet Sasmaz
Order of Authors:	Ahmet Sasmaz
	Pierpaolo Zuddas
	Marianna Cangemi
	Daniela Piazzese
	Gulsah Ozek
	Marco Venturi
	Paolo Censi
Abstract:	We investigated the distribution of Zr, Hf, and rare earth elements (REE) as the sum of lanthanides plus Y) in the hydrothermal system in the Lake Van area of south-eastern Turkey. This system is characterised by water with variable pH in alkaline conditions resulting from hydrothermal CO 2 upraise and neoformation of calcite minerals in near equilibrium with the interacting waters. Zr, Hf, and REE determinations were carried out for aqueous phases and suspended solids in lake water and surrounding thermal springs. We found that dissolved Hf is partitioned relative to Zr during calcite formation and that such fractionation is a function of the Ca 2+ activity in warm water. The observed Zr-Hf fractionation is explained by coulombic interactions that occur between suspended solid particles and dissolved phases at the calcite-water interface. There, the surfaces of carbonate minerals demonstrated greater reactivity towards aqueous Hf-bearing species relative to Zr-complexes. This evidence involves a coulombic mechanism of reactivity at the calcite-water interface because Hf complexes are negatively charged while Zr compounds are uncharged. Thus, authigenic calcite can behave as a suitable host for dissolved metal ion species to adsorb on crystal surfaces to remediate waste waters from mine drainage.
Suggested Reviewers:	Thomas H Darrah darrah.24@osu.edu Geochemist with a large experience in REE
	Rosa Cidu cidur@unica.it
	Johan Varekamp jvarekamp@wesleyan.edu lake geochemist
	Yigal Erel yerel@vms.huji.ac.il Trace element geochemist with a large experience in solid-water interface reactions
Response to Reviewers:	Response to Reviewer 1 Line 41 – the reference was added Line 73 – Yes, this problem was considered but sampling conditions in the studied areas and the limited time elapsed between the sample collection and filtration allowed us to filter waters under clean lab conditions.

	Line 131 – only two significant digits were reported in Eh values. Line 193 – allo scopo di riportare le concentrazioni disciolte sempre in pmol/L alcuni valori maggiori di 1000 pmol/L erano stati riportati con la virgola (1,000) per dividere le migliaia dalle altre cifre intere. Per evitare confusione nel lettore questa scelta è stata evitata. Response to Reviewer 2 A brief geological summary of the lake Van area was added. Line 31 – done Line 37 – two references were added. Line 45 – the text was corrected Line 97 – w/w concentrations of HNO3, NH4OH and HCl solutions and the mark ULTREX II of Baker chemicals were added. Line 140-142 – data are in weight %. They were assessed with the Rietveld method as reported at lines 115-120. Line 198 – the correct text is “without evidence of a positive Ce anomaly”. Positive was lost. Sorry! Line 241 –in lines 243-247, we list several minerals (Fe-oxyhydroxides, Phosphates, Salt minerals, sulphates) that can fractionate MREE relative to other REE. It is a large and heterogeneous group of minerals where it is hard to identify a possible MREE source during rock-water interactions. Probably MREE fractionation in a so large group of minerals is a process ruled by crystal-chemical reasons since elements from Sm to Dy show similar ionic radii than Ca2+ and Na+. Then, the text is limited to suggest possible minerals representing reasonable MREE sources. Fig. 3. It was modified Fig. 4. It was modified Fig. 5. pCa = -Log[Ca2+]. [Ca2+] is expressed in mol/L, as reported in the caption. Table 1. The number of digits was modified. Table 2. No. Those reported in Table 2 is the mineralogical composition expressed in weight % units. These are measured with the TOPAS software carrying out on X-ray spectra according to the Rietveld method (see Materials and Methods chapter). Supplementary tables have been corrected as suggested by the reviewer.

Zirconium and hafnium fractionation and distribution of Rare Earth Elements in neutral–alkaline waters: Case study of Lake Van hydrothermal system, Turkey

Sasmaz A.[1], Zuddas P.[2], Cangemi M.[3], Piazzese D.[3], Ozek G.[1], Venturi M.[4], Censi P.[3*]

1. Firat University, Geological Engineering, 23119, Elazig (Turkey)
2. Sorbonne Université, CNRS, METIS - 4, Rue Jussieu, F75005, Paris (France)
3. University of Palermo, DiSTeM, Via Archirafi 22, 90123, Palermo (Italy)
4. SIDERCEM S.R.L., Via Libero Grassi 7, 93100 Caltanissetta (Italy).

• corresponding author paolo.censi@unipa.it +393479662844

Abstract

We investigated the distribution of Zr, Hf, and rare earth elements (REE) as the sum of lanthanides plus Y) in the hydrothermal system in the Lake Van area of south-eastern Turkey. This system is characterised by water with variable pH in alkaline conditions resulting from hydrothermal CO_2 upraise and neoformation of calcite minerals in near equilibrium with the interacting waters. Zr, Hf, and REE determinations were carried out for aqueous phases and suspended solids in lake water and surrounding thermal springs. We found that dissolved Hf is partitioned relative to Zr during calcite formation and that such fractionation is a function of the Ca^{2+} activity in warm water. The observed Zr-Hf fractionation is explained by coulombic interactions that occur between suspended solid particles and dissolved phases at the calcite-water interface. There, the surfaces of carbonate minerals demonstrated greater reactivity towards aqueous Hf-bearing species relative to Zr-complexes. This evidence involves a coulombic mechanism of reactivity at the calcite-water interface because Hf complexes are negatively charged while Zr compounds are uncharged. Thus,

authigenic calcite can behave as a suitable host for dissolved metal ion species to adsorb on crystal surfaces to remediate waste waters from mine drainage.

Keywords

Zr/Hf ratio; REE; Alkaline lakes; Turkey

1 Introduction

Zirconium, Hf, and rare-earth elements (REE) ~~REEs~~ are used in specialised technology industries notwithstanding their limited production (Chakhmouradian and Wall, 2012; Jones III et al., 2017). Demand for these elements is high leading an effort by the mineral exploration industry to understand genetic processes and discover new resources. Geochemically, these elements were considered to be 'immobile' in subsurface conditions while some works indicate easy water transport under subsurface hydrothermal conditions~~.~~ (Michard and Albarede, 1986; Michard, 1989). Accordingly, REE enrichment has been observed in deposits formed from carbonisation in alkaline environments where Zr concentrations were enriched by a factor of 3 to 4 (Estrade et al., 2015). The behaviour of these strategic elements under surface and subsurface conditions is often neglected because of difficulties in accurate analytical determination at the level of pmol/kg in natural water. In a recent survey, the dissolved Zr/Hf ratio was different from that found in the rock minerals (Censi et al., 2020; Cidu et al., 2013; Inguaggiato et al., 2015, 2016; Parisi et al., 2017; Tepe and Bau, 2015; Zuddas et al., 2017, 2018) suggesting that the subsurface cycle is important in the accumulation of these elements. In fact, the Zr/Hf molar value in rock minerals was 71.4±5.6 which corresponds to the so-called 'chondritic' signature (Jochum et al., 1986), while natural water had a wider range of Zr/Hf (Zuddas et al., 2018). The supergene geochemical cycle of Zr and Hf participates in the accumulation and stability of these elements through the process of dissolution and precipitation of the minerals. Because the composition of subsurface and surface waters is often near equilibrium with carbonate minerals like calcite, calcite is expected to play a significant role in the supergene behaviour of these elements. Although carbonates are among the most common minerals in equilibrium with natural water, the formation of neogenic calcite also determined the change in REE distribution observed by Moller and De Lucia (2020) in controlled laboratory investigations. To explain Zr-Hf decoupling during calcite crystallisation and the concurrent behaviour of REEs, we investigated the distribution of these elements in a natural hydrothermal system characterised by the formation of calcite under the neutral and alkaline water system found at

Lake Van and characterised by low thermal and lake waters with pH ranging from 6 to 10, resulting from a variable CO_2 flux (Degens and Kurtman, 1978; Moller and Bau, 1993). The Lake Van system is characterised by neogenic precipitation in the form of Ca-Mg carbonates (Moller and Bau, 1993).

2 Material and Methods

Lake Van is located in south-eastern Turkey (Fig. 1) which formed during the collision between European and Arabian plates. The sequence starts with Paleozoic metamorphic rocks overlaid by Permian limestones and schists followed by sediments of marine and continental origin (Upper Cretaceous-Pliocene) closed by basic and felsic volcanic-pyroclastic rocks (Oligocene-Recent) (Degens and Kurtman, 1978, Yilmaz, 1990). Heat flow data suggest the presence of a magmatic body beneath the lake bottom, possibly related to Nemrut Volcano and sustaining input of CO_2 into Lake Van waters (Moller and Bau, 1993). Presently, the Lake Van represents the largest soda lake worldwide resulting from a combined volcanogenic hydrothermal CO_2 input and seasonal evaporitic conditions (Moller and Bau, 1993).

Formatted: Indent: First line: 0.39"

Formatted: Font: Not Bold

2.1 Field sampling

Lake Van is located in south-eastern Turkey (Fig. 1) which formed during the collision between European and Arabian plates. Field study and water sampling were conducted in November 2018 and consisted of a 16 samples collected from lake water and thermal springs. Coordinates and geologic units of the collected samples are given in Table 1. Lake water was sampled at a depth of 15–20 cm. Physicochemical parameters (pH, redox potential (Eh), temperature, and electrical conductivity) were measured with an Eh oxytrode Pt probe (Hamilton™) using a standard reference solution buffer at 0.475±0.005 V~~475±5 mV~~. Accuracy of determinations was ±10 mV. For the major ion determinations, water samples were filtered in the field through 0.45 µm Millipore® cellulose acetate filters into 50 mL polyethylene bottles and acidified with ultrapure HNO_3. Water samples for trace and rare element analyses were collected in 2,000 mL Nalgene bottles at each sampling site.

2.2 Water analysis and thermodynamic modelling

In the laboratory, samples were filtered (Millipore® manifold filter, 47 mm diameter with a 0.45 µm pore size cellulose nitrate membrane), then 5% ultrapure HNO_3 acid solution was added to reach pH ≈ 2. Zirconium, Hf, and REEs in aqueous samples were analysed according to the methods of Raso et al. (2013). Briefly, an excess of $FeCl_3$ (1%) solution was added to each sample (1 L), and a suitable volume of NH_4OH (25%) solution was added to attain a pH of 8 to induce precipitation of solid $Fe(OH)_3$. During this process, Zr, Hf, and REEs were held onto the surface of the crystallising solid. To ensure that crystallisation of $Fe(OH)_3$ was complete, the solution was left in a closed flask for 48–72 h in a stirrer. Next, the iron concentration was measured to assess recovery and was consistently greater than 95%. Precipitated $Fe(OH)_3$, together with Zr, Hf, and REEs, was collected on a membrane filter (Millipore® manifold filter, 47 mm diameter with 0.45 µm pore size). The solid filtrate was then dissolved in 3 M HCl, and the obtained solution was diluted to 1 M HCl prior to analysis using a Quadrupole-ICP-MS (Agilent 7800 series) with an external calibration procedure. The overall strategy and a detailed evaluation of the analytical errors were reported in Raso et al. (2013). The overall enrichment factor measured for Zr, Hf, and REE concentrations corresponded to 66.7.

Lanthanum, Ce, and Eu anomalies were calculated using eqations 1–3 (Alibo and Nozaki, 1999):

$$\frac{La}{La^*} = \frac{[La]_n}{3*[Pr]_n+2*[Nd]_n}, \quad (1)$$

$$\frac{Ce}{Ce^*} = \frac{2*[Ce]_n}{[La]_n+[Pr]_n}, \text{ and} \quad (2)$$

$$\frac{Eu}{Eu^*} = \frac{2*[Eu]_n}{[Sm]_n+[Gd]_n}, \quad (3)$$

where the subscript n indicates shale-normalised elemental concentrations calculated relative to the Post Archean Australian Shale (PAAS, Taylor and McLennan, 1995).

All chemicals used during laboratory manipulations were ultrapure grade. Ultrapure water (resistivity of 18.2 MΩ cm or better) was obtained from an Arium® mini system (Sartorius, Italy). Nitric acid 65% (w/w), NH_4OH (20%) and HCl (30%) solutions ~~ammonia solution, and HCl acid~~

were purchased from J.T. Baker (ULTREX II) chemicals. Working standard solutions of the elements studied were prepared daily by stepwise dilution of standard multi-element stock solutions from DBH, Merck, or CPI International (1,000±5 mg/L) in a 1 M HCl medium. All labware was polyethene, polypropylene, or Teflon® and the calibration of all volumetric equipment was verified. Assessment of the analytical precision of Zr, Hf, and REEs was performed on five aliquots (500 mL each) of NASS-6 (seawater certified reference material for trace metals) distributed by the National Research Council of Canada. These certified reference materials were treated as water samples according to the procedure mentioned above and the concentrations obtained were compared with those previously reported by Raso et al. (2013) and Lemaitre et al. (2014). Analysed values are reported in Supplementary Data 1.

Thermodynamic modelling of the chemical composition of the water performed was using PHREEQC software and adding additional Lawrence Livermore National Laboratory (LLNL) database (version 3.0.6, Parkhurst and Appelo, 2010).

2.3 Suspended solids

X-ray diffraction investigations were carried out with a Philips PW14 1373 X-ray spectrometer (Cu-Kα radiation 2Θ range 10–40°, step size 0.02°, and a 1-min step time). The X-ray spectra were analysed by the Rietveld method (Program DiffracPlus TOPAS®, Version 4.0, Bruker AXS Inc., Karlsruhe, Germany) using parameters for the Rietveld refinement method obtained from the Inorganic Crystal Structure Database (ICSD) program. This method consists of fitting the experimental XRD spectrum to the theoretical spectrum (Young, 1993). A detailed explanation of the method is reported in Scarlett and Madsen (2006).

Scanning electron microscopy (SEM) of suspended particles was carried out on materials collected after filtration onto cellulose nitrate membranes. Dried solids were mounted on an aluminium stub and gold coated. The SEM analyses were carried out using a LEO 440 SEM equipped with an EDS system OXFORD ISIS Link and Si (Li) PENTAFET detector at the SIDERCEM SRL laboratory (Caltanissetta, Italy). Chemical analyses were carried out by digesting 100 mg of each sample in 10

mL of a 1:1 HNO_3:H_2O_2 mixture in a sealed Teflon® TFM bomb using a microwave oven (CEM MARS 5 device). After digestion, the TFM bomb was rinsed, and the solution was filtered onto previously acid-cleaned 0.45 µm Millipore® filters to remove silicate residue. The filtered solution was diluted to 50 mL and stored for chemical analyses.

3 Results and Discussion

3.1 System description

The concentration of major elements, pH, Eh, electric conductivity, and temperature are reported in the Supplementary Data 2. Water samples had ionic strength ranging from 0.024 to 0.222 M in thermal water and between 0.004 and 0.443 M in lake water. Thermal water had pH between 5.8 and 7.1 and Eh between 0.01~~3~~ and 0.17~~2~~ V, while lake water had pH between 8 and 10 and Eh from -0.2~~988~~ and 0.01~~2~~ V. Figure 2a shows that lake water preferentially falls in the field of alkaline elements (only two samples have higher Ca^{2+} and Mg^{2+}concentrations) while thermal water fell between alkaline and Ca^{2+}-rich field (few samples fell in the Mg^{2+} corner).

The SEM images of the suspended particulates revealed that suspended particulate matter in lake water consisted of authigenic carbonates associated with biogenic detritus and lithic fragments (Fig. 3a-f), while suspended solids in thermal waters were authigenic carbonates and Fe-rich particles and lithogenic fragments (Fig. 3g-i). Iron-bearing particulates in the samples were often mixed with authigenic calcite and dolomite (see elemental maps in Fig. 3i). The X-ray diffraction analyses confirmed the presence of carbonate minerals identified as calcite and low-Mg calcite representing up to 80% of the authigenic minerals (Table 2). Other phases collected were Fe-oxyhydroxides and detritic silicate particles reaching 10–15% of the total mass.

Using the chemical composition of the collected samples, we estimated the saturation state with respect to the mineral in equilibrium and found both lake water and thermal water were saturated or oversaturated with respect to calcite or low-Mg calcite. Some water was also saturated with respect to dolomite and goethite in agreement with the results of the X-ray determinations of the collected suspended matter.

3.2 Zr and Hf behaviour

Zr and Hf concentrations in both aqueous and suspended particulate matter are reported in Supplementary Data 3 and 4, respectively. In the aqueous phase, the concentration of Zr and Hf was not homogenous. Lake waters had Zr concentrations between 79 and 4~~,~~958 pmol/L while Hf concentrations fell between 2 and 53 pmol/L, and thermal waters had Zr concentrations between 32 and 1.4~~25~~ pmol/L; whereas Hf concentrations fell between 0.5 and 14 pmol/L. The concentrations of Zr and Hf in thermal waters were 1 to 3 orders of magnitude lower than those found in lake water; however, the concentration of Zr as a function of Hf was linearly correlated with an intercept equal to zero and parametrising a single slope of 90~~.4~~±2~~1.7~~ (Fig. 4a). This value was higher than the Zr/Hf value of 71±~~5.~~6 for crustal materials and chondrites (Jochum et al., 1986) indicating that the calcite precipitation fractionates the Zr/Hf ratio in water. In the suspended solids from lake water, Zr concentration ranged from 99~~.5~~ to 2~~,~~533~~.2~~ nmol/kg, whereas Hf fell between 2.6 and 77.1 nmol/kg. Suspended solids from thermal water had Zr concentrations between 20.7 and 346.7 nmol/kg and Hf between 0.6 and 6.8 nmol/kg. Similarly, Zr and Hf in solids collected from thermal water were lower compared to suspended solids found in lake water. Figure 4B shows the concentration of Zr as a function of Hf in neogenic calcite from lake water and describes a linear slope of 33.5 similar to calcite in equilibrium with thermal water where the slope was 37.

These results show that the Zr/Hf ratio in water is different from that in crustal rocks and that Hf is preferentially enriched in authigenic carbonate minerals. Preferential enrichment of Hf relative to Zr in newly-formed suspended carbonates was unexpected and may result from processes occurring at the surface-water interface. The calcite-water interface is generally represented by an electric double-layer of weak mineral solubility buffered by CO_3^{2-} ions with the ζ potential of the {104} carbonate surface independent of pH (Herberling et al., 2011). Laboratory measurements indicate the positive surface potential (up to 24 mV) when the Ca^{2+} concentration in solution is between 10^{-2} and 10^{-4} M (Al-Mahrouqui et al., 2017). Byrne (2002) made a critical review of stability constants for Zr and Hf hydroxyl complexes based on the work of Sillen and Martell (1964),

Baes and Mesmer (1976), Ekberg et al. (2004), and Brown et al. (2005) and estimated that the most abundant Zr and Hf complexes in aqueous phase were $[Zr(OH)_4]^0$ and $[Hf(OH)_5]^-$, respectively (Koschinsky and Hein, 2003). Reporting Zr/Hf ratios as a function of pCa:

$$pCa = -Log(a_{Ca^{2+}}) (4)$$

~~(pCa= log[Ca^{2+}])~~ (Fig. 5), we found two distinct correlation lines, one for thermal water and one for lake water, suggesting that negatively-charged $[Hf(OH)_5]^-$ complexes were preferentially scavenged onto {104} positive carbonate surfaces and were, in turn, removed from the aqueous phase. This potential mechanism explains the Zr/Hf fractionation observed during calcite precipitation under pH conditions between 7 and 10 and should correspond to the higher binding energy between Hf and {104} calcite surface relative to Zr as estimated by theoretical ab initio calculations (Pinto et al., 2017). Our results support the Zr/Hf fractionation observed by Firdaus et al. (2011, 2018) during Fe-oxyhydroxide formation. Fe-oxyhydroxide was in fact positively charged under weak alkaline conditions (Koschinsky and Hein, 2003). On the contrary, Zr-Hf fractionation did not occur onto surfaces of Mn-oxyhydroxides that were negatively charged at the pH up to acidic values (Tripathy et al., 2001). The Zr-Hf fractionation here observed during calcite formation and interpreted as water-interface interaction is consistent with the Zr-Hf fractionation found in stromatolites (Censi et al., 2015), halite (Censi et al., 2017a, 2020), and other groundwater environments (Censi et al., 2017b; Inguaggiato et al., 2015, 2016).

3.3 REE behaviour

Dissolved REE concentrations in lake water and thermal water in the Lake Van system ranged between 7~~,~~135 and 76~~,~~140 pmol/L and from 168 to 17~~,~~426 pmol/L, respectively (Supplementary Data 3). In lake waters the shale normalised pattern (Fig. 6a~~A~~) reveals the presence of La positive anomaly as well an 'ascending' feature leading to enrichment in heavy REE (HREE, from Ho to Lu) while thermal waters have a single slight medium REE (MREE, from Sm to Dy) enrichment (Fig. 6b~~B~~). In both types of water, Eu anomalies were 0.3 and 4.8 without evidence of a positive Ce anomaly ($0.1 \leq Ce/Ce^* \leq 1$). The progressive increase of REEs observed in the

Formatted: Indent: First line: 0"

normalised patters in these waters may result from the values of the stability constants of di-carbonate and carbonate REE-complex ions (Lee and Byrne, 1993; Liu and Byrne, 1998) potentially producing $[REE(CO_3)_2]^-$ complexes (Johannesson et al., 1994; Johannesson and Lyon, 1994; Kerrich et al., 2002; Moller and Bau, 1993). Our data showed a higher abundance of La and therefore inconsistent with earlier REE measurements from Van Lake waters (Moller and Bau, 1993). The water level of Lake Van has dropped due to climate change over the last 30 years while the input of lithogenic solids increased. The main difference between the REE distribution recognised in lake Van waters and that reported by Moller and Bau (1993) is the lack of positive Ce anomaly in our samples. This may be caused by a larger dissolution of lithogenic particles typical of continental and coastal waters. The dissolution of lithogenic solids usually provides La enrichment in the aqueous phase that can conceal the concurrent Ce enrichment completely or partially (Censi et al., 2007; Greaves et al., 1999; Grenier et al., 2018).

Suspended particulate material collected from the lake and thermal waters had a total concentration of REEs ranging between 508.2 and 835.2 nmol/kg and from 102.3 to 278.5 nmol/kg, respectively (Supplementary Data 4). These values are 3 to 4 orders of magnitude higher than the concentrations found in related waters. The shale-normalised REE patterns of suspended calcites collected in lake waters (Fig. 6c) and thermal waters (Fig. 6d) display positive Ce anomalies ranging from 1.1 to 3.1, an enrichment in MREEs with positive Eu anomalies ($0.8 < Eu/Eu^* < 4.2$), and slight progressive depletion of HREEs. Suspended solids from thermal waters showed 'bulged' REE patterns (Fig. 6d~~D~~) while solids from lake waters had flatter patterns (Fig. 6C). The REE distribution in shale-normalised patterns usually show MREE enrichment mainly ruled by crystal-chemical reasons, as demonstrated by the review of distribution coefficient values reported by Moller and De Lucia (2020). In suspended solids from thermal water, the MREE enrichment was more evident than in materials collected from lake water. This evidence is probably justified by the concurrent presence of a detrital fraction in the 'bulge' of suspended solids from lake water with a 'flatter' shale-like trend in the normalised concentration (Taylor and McLennan, 1988).

The behaviour of Y-Ho twin is different in lake and thermal waters. In lakes, Y and Ho concentrations ranged from 3,845 to 62,279 pmol/L and 36 to 686 pmol/L respectively, whereas in thermal springs, Y ranges up to 3,577 pmol/L, whereas Ho fell between 2 and 68 pmol/L. The related Y/Ho ratios spanned from 51 to 111 in lake water and between 53 and 162 in thermal water. These ratios fell between chondritic and super-chondritic values. On the contrary, in carbonates from suspended solids, the Y/Ho ratio ranged from 32.4 to 49.6 in lake water and from 28.6 and 47.8 in thermal water. Then Y/Ho values in suspended solids spanned between slight subchondritic to chondritic values (Y/Ho = 52±5.1, Jochum et al., 1986).

The role played by the formation of calcite in the distribution of REEs in alkaline waters was highlighted by the super-chondritic value of the Y/Ho ratio. Our study revealed that Ho was 2 to 3 orders of magnitude higher than Y during calcite formation causing enrichment. The preferential enrichment of Ho in calcite compared to Y observed in our study may reflect the larger value of the Misono softness parameter of Ho^{3+} relative to Y^{3+} (Thompson et al., 2013) due to the different external electronic configuration of these metal ions (Qu et al., 2009).

The different fractionation of these elements found during the formation of calcite also reflects other processes. In thermal water, the intensity of the water-rock interaction may cause MREE enrichment (Fig. 6c). Dissolution of lithogenic rocks may be the source of MREE (Bau, 1999; Censi et al., 2019; Greaves et al., 1999; Haley et al., 2004; Inguaggiato et al., 2016; Lin et al. 2019) and explain MREE enrichment observed in authigenic hydrothermal carbonates (Jakubowicz et al., 2015; Phan et al., 2019; Wang et al., 2020), phosphates (Censi et al., 2007; Hannigan and Sholkovitz, 2001; Reynard et al., 1999; Zhang et al., 2016), sulphates (Censi et al., 2014; 2018; Kagi et al., 1993; Playà et al., 2007; Toulkeridis et al., 1998), and Fe-oxyhydroxides (Bau, 1999; Davranche et al., 2011).

4 Implications and Conclusions

The results of our investigation of water oversaturated with calcite indicate that calcite plays a crucial role in constraining Zr-Hf fractionation and the geochemical behaviour of REEs in alkaline

lake waters. The strong reactivity of positively charged {104} surfaces of calcite coupled with the aqueous Zr and Hf speciation lead to preferential accumulation of Hf in calcite relative to Zr. This indication agrees with the larger affinity of Hf towards solid surfaces relative to Zr already evidenced onto the surfaces of Fe-oxyhydroxides. But the Hf removal onto the carbonate surfaces is ruled by pCa, whereas onto the Fe-oxyhydroxide surfaces is ruled by pH. Therefore, changes of the Zr/Hf ratio in natural waters relative to the chondritic signature indicate that these elements are involved in processes occurring at the interface with crystallising authigenic minerals.

Differences in the external electronic configuration of Zr and Hf is similar to that between Y and Ho due to differences in softness/hardness between Zr and Hf and between Y and Ho that, in turn, influence hydrolysis during formation of Zr and Hf hydroxyl complexes. This process could be a crucial aspect of the fractionation of these metal ions during calcite formation. Differences in softness between Y and Ho lead increase stability of Ho-O relative to Y-O bonds on solid surfaces and rule Y-Ho fractionation at the solid-liquid interface.

Based on previous researches addressed to the larger Hf affinity relative to Zr towards crystal surfaces of halite, potash salts and Fe-oxyhydroxides, this study contributes to demonstrate that the larger surface reactivity of Hf relative to Zr is a widespread phenomenon through the sedimentary processes. The evidence of this phenomenon is detected measuring the Zr/Hf ratio in natural waters and in authigenic minerals.

ACKNOWLEDGMENT

This research was partially funded by the contracts CORI 2017 (University of Palermo) and CON-0037 funded by the SIDERCEM S.R.L. - University of Palermo Agreement and The Science and Technological Research Council of Turkey (TUBITAK 118Y319).

287 REFERENCES

288 Al-Mahrouqi, D.A., Vinogradov, J., Jackson, M.D., 2017. Zeta potential of artificial and natural
289 calcite in aqueous solution. Adv. Colloid. Interface Sci. 240, 60-76.
290 Alibo, D.S., Nozaki, Y., 1999. Rare earth elements in seawater: Particle association, shale-
291 normalization, and Ce oxidation. Geochim. Cosmochim. Acta 63, 363-372.
292 Baes, C. F., Mesmer R. S. 1976. The Hydrolysis of Cations. John Wiley & Sons, Ltd, New York,
293 London, Sydney, Toronto.
294 Bau, M., 1999. Scavenging of dissolved yttrium and rare earths by precipitating iron oxyhydroxide:
295 Experimental evidence for Ce oxidation, Y-Ho fractionation, and lanthanide tetrad effect.
296 Geochim. Cosmochim. Acta 63, 67–77.
297 Brown, P.L., Curti, E., Grambow, B. Chemical Thermodynamics of Zirconium, Mompean J. P.,
298 Perrone J. (eds.) NEA Data Bank, OECD 2005, pp 512.
299 Byrne, R.H., 2002. Inorganic speciation of dissolved elements in seawater: The influence of pH on
300 concentration ratios. Geochem. T. 3, 11-16.
301 Censi, P., Cangemi, M., Brusca, L., Madonia, P., Saiano, F., Zuddas, P., 2015. The behaviour of
302 rare-earth elements, Zr and Hf during biologically-mediated deposition of silica-stromatolites and
303 carbonate-rich microbial mats. Gondwana Res. 27, 209-215.
304 Censi, P., Inguaggiato, C., Chiavetta, S., Schembri, C., Sposito, F., Censi, V. and Zuddas, P. (2017a)
305 The behaviour of zirconium, hafnium and rare earth elements during the crystallisation of halite
306 and other salt minerals. Chem Geol 453, 80-91.
307 Censi, P., Raso, M., Saiano, F., Zuddas, P., Oliveri, E., 2019. Zr/Hf ratio and REE behaviour: A
308 coupled indication of lithogenic input in marginal basins and deep-sea brines. Deep-Sea Res. Pt II
309 164, 216-223.
310 Censi, P., Raso, M., Yechieli, Y., Ginat, H., Saiano, F., Zuddas, P., Brusca, L., D'Alessandro, W.,
311 Inguaggiato, C., 2017b. Geochemistry of Zr, Hf, and REE in a wide spectrum of Eh and water

composition: the case of Dead Sea Fault system (Israel). Geochem., Geophys., Geosyst. 18, 844-857.

Censi, P., Saiano, F., Zuddas, P., Nicosia, A., Mazzola, S., Raso, M., 2014. Authigenic phase formation and microbial activity control Zr, Hf, and rare earth element distributions in deep-sea brine sediments. Biogeosciences 11, 1125–1136.

Censi, P., Sirota, I., Zuddas, P., Lensky, N., Merli, M., Saiano, F., Piazzese, D., Sposito, F., Venturelli, M., 2020. Trace element fractionation through halite crystallisation. Geochemical mechanisms and environmental implications, Sci. Total Environ. 723, art. 137926

Censi, P., Sposito, F., Inguaggiato, C., Zuddas, P., Inguaggiato, S., Venturi, M., 2018. Zr, Hf and REE distribution in river water under different ionic strength conditions. Sci. Total Environ. 645, 837-853.

Censi, P., Sprovieri, M., Saiano, F., Di Geronimo, S.I., Larocca, D., and Placenti, F. (2007). The behaviour of REEs in Thailand's Mae Klong estuary: Suggestions from the Y/Ho ratios and lanthanide tetrad effects. Estuarine, Coastal and Shelf Science 71(3-4), 569-579.

Chakhmouradian, A.R., Wall, F., 2012. Rare earth elements—Minerals, mines, magnets (and more): Elements 8, 5, 333–340.

Cidu R., Vittori Antisari L., Biddau R., Buscaroli A., Carbone S., Da Pelo S., Dinelli E., Vianello G., Zannoni D., 2013. Dynamics of rare earth elements in water-soil systems: the case study of the Pineta San Vitale (Ravenna, Italy). Geoderma 193-194: 52-67.

Davranche M, Grybos M, Gruau G, Pedrot M, Dia A, Marsac R (2011) Rare earth element patterns: a tool for identifying trace metal sources during wetland soil reduction. Chem Geol 284:127–137

Degens, E.T., Kurtman, F., Eds. The Geology of Lake Van, Min. Res. Explor. Inst. Turkey, Ankara, 1978, pp. 158.

Ekberg, C., Källvenius, G., Albinsson, Y., Brown, P.L., 2004. Studies on the hydrolytic behavior of zirconium (IV). J. Solution Chem. 33, 47-79.

Estrade G., Salvi, S., Béziat, D., Williams-Jones, A.E., 2015. The Origin of Skarn-Hosted Rare-Metal Mineralization in the Ambohimirahavavy Alkaline Complex, Madagascar. Economic Geology, v. 110, pp. 1485–1513.

Firdaus, M.L., Mashio, A.S., Obata, H., McAlister, J.A., Orians, K.J., 2018. Distribution of zirconium, hafnium, niobium and tantalum in the North Atlantic Ocean, north-eastern Indian Ocean and its adjacent seas, Deep-Sea Res. Pt I 140, 128-135.

Firdaus, M.L., Minami, T., Norisuye, K., Sohrin, Y. 2011. Strong elemental fractionation of Zr-Hf and Nb-Ta across the Pacific Ocean. Nat. Geosci. 4, 227–230.

Greaves, M.J., Elderfield, H., Sholkovitz, E.R., 1999. Aeolian sources of rare earth elements to the Western Pacific Ocean. Mar. Chem. 68 (1–2), 31–38.

Grenier, M., Garcia-Solsona, E., Lemaitre, N., Trull, T.W., Bouvier, V., Nonnotte, P., Beek, P., Souhaut, M., Lacan, F., Jeandel, C., 2018. Differentiating lithogenic supplies, water mass transport, and biological processes On and Off the Kerguelen Plateau using rare earth element concentrations and neodymium isotopic compositions. Frontiers in Marine Science, 5 (NOV), art. no. 426.

Haley, B.A., Klinkhammer, G.P., McManus, J., 2004. Rare earth elements in pore waters of marine sediments. Geochim. Cosmochim. Acta 68, 1265–1279. http://dx.doi.org/10.1016/j.gca.2003.09.012.

Hannigan, R. E., Sholkovitz E. R., 2001. The development of middle rare earth element enrichments in freshwaters: Weathering of phosphate minerals, Chem. Geol., 175, 495-508.

Herberling, F., Trainor, T.P., Lützenkirchen, J., Eng, P., Deneke, M.A., Bosbach, D., 2011. Structure and reactivity of the calcite–water interface. J. Coll. Inter. Sci. 354, 843-857.

Inguaggiato, C., Censi, P., Zuddas, P., D'Alessandro, W., Brusca, L., Pecoraino, G., Bellomo, S., 2016. Zirconium-hafnium and rare earth element signatures discriminating the effect of atmospheric fallout from hydrothermal input in volcanic lake water. Chem. Geol. 433, 1–11.

Inguaggiato, C., Censi, P., Zuddas, P., Londono, J.M., Chacon, Z., Alzate, D., Brusca, L., D'Alessandro, W., 2015. Geochemistry of REE, Zr and Hf in a wide range of pH and water composition: the Nevado del Ruiz volcano-hydrothermal system (Colombia). Chem. Geol. 417, 125–133.

Jakubowicz, M., Dopieralska, J., Belka, Z., 2015. Tracing the composition and origin of fluids at an ancient hydrocarbon seep (Hollard Mound, Middle Devonian, Morocco): A Nd, REE and stable isotope study. Geochim. Cosmochim. Acta 156, 50-74.

Jochum, K.P., Seufert, H.M., Spettel, B., Palme, H., 1986. The solar-system abundances of Nb, Ta, and Y, and the relative abundances of refractory lithophile elements in differentiated planetary bodies. Geochim. Cosmochim. Acta 50, 1173-1183.

Johannesson, K.H., Lyons, W.B., 1994. The rare earth element geochemistry of Mono Lake water and the importance of carbonate complexing. Limnology and Oceanography 39 (5), pp. 1141-1154.

Johannesson, K.H., Lyons, W.B., Bird, D.A., 1994. Rare earth element concentrations and speciation in alkaline lakes from the western U.S.A. Geophysical Research Letters 21, 773-776.

Jones, J.V., III, Piatak, N.M., and Bedinger, G.M., 2017, Zirconium and hafnium, chap. V of Schulz, K.J., DeYoung, J.H., Jr., Seal, R.R., II, and Bradley, D.C., eds., Critical mineral resources of the United States—Economic and environmental geology and prospects for future supply: U.S. Geological Survey Professional Paper 1802, p. V1– V26, https://doi.org/10.3133/pp1802V.

Kagi, H., Dohmoto, Y., Takano, S. and Masuda, A., 1993. Tetrad effect in lanthanide partitioning between calcium sulphate crystal and its saturated solution. Chem. Geol. 107, 71-82.

Kerrich, R., Renaut, R.W., Bonli, T., 2002. Trace-element composition of cherts from alkaline lakes in the east African rift: a probe for ancient counterparts. Spec. Publ. 73, 277–298.

Koschinsky, A., Hein, J.R., 2003. Uptake of elements from seawater by ferromanganese crusts: Solid-phase associations and seawater speciation. Mar. Geol. 198, 331-351.

Lee J.H., Byrne R. H. (1993). Complexation of trivalent rare earth elements (Ce, Eu, Gd, Tb, Yb) by carbonate ions. Geochim. Cosmochim. Acta 57, 295–302.

Lemaitre, N., Bayon, G., Ondréas, H., Caprais, J.C., Freslon, N., Bollinger, C., Rouget M.-L., De Prunelé A., Ruffine L., Olu-Le Roy K., Sarthou G., 2014. Trace element behaviour at cold seeps and the potential export of dissolved iron to the ocean. Earth Planet. Sci. Lett. 404, 376-388.

Lin, J., Nilges, M.J., Wiens, E., Chen, N., Wang, S., Pan, Y., 2018. Mechanism of Gd^{3+} uptake in gypsum ($CaSO_4 \cdot 2H_2O$): Implications for EPR dating, REE recovery and REE behavior. Geochim. Cosmochim. Acta 258, 63-78.

Liu, X.W., Byrne, R.H., 1998. Comprehensive investigation of yttrium and rare earth element complexation by carbonate ions using ICP-mass spectrometry. J. Solution Chem. 27, 803-815.

Michard A.,1989. Rare earth systematics in hydrothermal fluids. Geochim. Cosmochim. Acta 53, 745–750.

Michard A., Albarede F., 1986. The REE contents of some hydrothermal fluds. Chem. Geol. 55, 51–60.

Moller, P., Bau, M. 1993. Rare-earth patterns with positive cerium anomaly in alkaline waters from Lake Van, Turkey. Earth Planet. Sci Lett. 117, 671-676.

Möller, P., De Lucia, M., 2020. Incorporation of rare earths and yttrium in calcite: A critical re-evaluation. Aquat. Geochem., 26 (2020), pp. 89-117

Parisi, M. G., Cammarata, I., Cammarata, M., Censi, V., 2017. Rare earths, zirconium and hafnium distribution in coastal areas: The example of Sabella spallanzanii (Gmelin, 1791). Chemosphere 185, 268-276.

Parkhurst, D.L., Appelo, C.A.J., 2010. User's Guide to PHREEQC (Version 2.17.5) - A Computer program for Speciation, Batch- Reaction, One-Dimensional Transport and Inverse Geochemical Calculations. Available at: http://www.brr.cr.usgs.gov/projects/ GWC_coupled/phreeqc/index.html.)

412 Phan, T.T., Hakala, J.A., Lopano, C.L., Sharma S., 2019. Rare earth elements and radiogenic
413 strontium isotopes in carbonate minerals reveal diagenetic influence in shales and limestones in
414 the Appalachian Basin. Chem. Geol. 509, 194-212.
415 Pinto, H., Haapasilta, V., Lokhandwala, M., Oberg, S., Foster, A.S., 2017. Adsorption and migration
416 of single metal atoms on the calcite (10.4) surface. J. Phys.-Condes. Mat. 29, (13)
417 Playà, E., Cendon, D.I., Trave, A., Chivas, A.R., Garcia, A., 2007. Non-marine evaporites with both
418 inherited marine and continental signatures: The Gulf of Carpentaria, Australia, at similar to 70
419 ka. Sed. Geol 201, 267-285.
420 Qu, C.L., Liu, G., Zhao, Y.F., 2009. Experimental study on the fractionation of yttrium from
421 holmium during the coprecipitation with calcium carbonates in seawater solutions. Geochem. J.
422 43, 403-414.
423 Raso, M., Censi, P., Saiano, F., 2013. Simultaneous determinations of zirconium, hafnium, yttrium
424 and lanthanides in seawater according to a co-precipitation technique onto iron-hydroxide.
425 Talanta 116, 1085–1090.
426 Reynard, B., Lécuyer, C., Grandjean, P., 1999. Crystal-chemical controls on rare-earth element
427 concentrations in fossil biogenic apatites and implications for paleoenvironmental
428 reconstructions. Chem. Geol. 155, 233-241.
429 Scarlett N.V.Y., Madsen I.C., 2006. Quantification of phases with partial or no known crystal
430 structures. Powder Diffraction 21, 278-284.
431 Sillen, L.G., Martell, A.E., 1964. Stability Constants of Metal–Ion Complexes, Special Publication
432 17, The Chemical Society, London, pp 754.
433 Taylor, S.R., McLennan, S.M., 1988. The significance of the rare earths in geochemistry and
434 cosmochemistry. Handbook on the Physics and Chemistry of Rare Earths, cap. 79, vol. 11, 485-
435 578.
436 Taylor, S.R., McLennan, S.M., 1995. The geochemical evolution of the continental crust. Rev.
437 Geophys. 33, 241–265.

Tepe, N., Bau, M., 2015. Distribution of rare earth elements and other high field strength elements in glacial meltwaters and sediments from the western Greenland Ice Sheet: evidence for different sources of particles and nanoparticles. Chem. Geol. 412, 59–68.

Thompson, A., Amistadi, M.K., Chadwick, O.A., Chorover, J., 2013, Fractionation of yttrium and holmium during basaltic soil weathering. Geochem. Cosmochim. Acta 119, 18-30.

Toulkeridis, T., Podwojewski, P., Clauer, N., 1998. Tracing the source of gypsum in New Caledonian soils by REE contents and S-Sr isotopic compositions. Chem. Geol. 145, 61-71.

Tripathy, S.S., Kanungo, S.B., Mishra, S.K., 2001. The electrical double layer at hydrous manganese dioxide/electrolyte interface. J. Colloid Interface Sci. 241, 112–119.

Wang, J.; Chang, J.; Li, C.; Han, Z.; Wang, T.; Han, H., 2020. Significance of Calcite Trace Elements Contents and C-O Isotopic Compositions for Ore-Forming Fluids and Gold Prospecting in the Zhesang Carlin-Like Gold Deposit of Southeastern Yunnan, China. Minerals 10, 338.

Yilmaz, Y., 1990. Comparison of young volcanic associations of western and eastern Anatolia formed under a compressional regime: a review. Jour. Volcan. Geoth. Res. 44, 69-87.

Young, R. The Rietveld Method, International Union of Crystallography, Oxford University Press, Oxford, 1993.

Zhang, L., Algeo, T.J., Cao, L., Zhao, L., Chen, Z.-Q., Li, Z., 2016. Diagenetic uptake of rare earth elements by conodont apatite. Palaeogeogr. Palaeoclimatol. Palaeoecol. 458, 176–197.

Zuddas, P., Censi, P., Inguaggiato, C., Sposito, F., 2018 The behaviour of zirconium and hafnium during water-rock interaction. Appl. Geochem. 94, 46–52.

Zuddas, P., Inguaggiato, C., Censi, P., D'Alessandro, W., 2017. Zr-Hf fractionation during water-rock interaction. Procedia Earth and Planetary Science 17, 670-673.~~Al-Mahrouqi, D.A., Vinogradov, J., Jackson, M.D., 2017. Zeta potential of artificial and natural calcite in aqueous solution. Adv. Colloid. Interface Sci. 240, 60-76.~~

~~Alibo, D.S., Nozaki, Y., 1999. Rare earth elements in seawater: Particle association, shale-normalization, and Ce oxidation. Geochim. Cosmochim. Acta 63, 363-372.~~

Baes, C. F., Mesmer R. S. 1976. The Hydrolysis of Cations. John Wiley & Sons, Ltd, New York, London, Sydney, Toronto.

Bau, M., 1999. Scavenging of dissolved yttrium and rare earths by precipitating iron oxyhydroxide: Experimental evidence for Ce oxidation, Y-Ho fractionation, and lanthanide tetrad effect. Geochim. Cosmochim. Acta 63, 67–77.

Brown, P.L., Curti, E., Grambow, B. Chemical Thermodynamics of Zirconium, Mompean J. P., Perrone J. (eds.) NEA Data Bank, OECD 2005, pp 512.

Byrne, R.H., 2002. Inorganic speciation of dissolved elements in seawater: The influence of pH on concentration ratios. Geochem. T. 3, 11-16.

Censi, P., Cangemi, M., Brusca, L., Madonia, P., Saiano, F., Zuddas, P., 2015. The behaviour of rare-earth elements, Zr and Hf during biologically-mediated deposition of silica-stromatolites and carbonate-rich microbial mats. Gondwana Res. 27, 209-215.

Censi, P., Inguaggiato, C., Chiavetta, S., Schembri, C., Sposito, F., Censi, V. and Zuddas, P. (2017a) The behaviour of zirconium, hafnium and rare earth elements during the crystallisation of halite and other salt minerals. Chem Geol 453, 80-91.

Censi, P., Raso, M., Saiano, F., Zuddas, P., Oliveri, E., 2019. Zr/Hf ratio and REE behaviour: A coupled indication of lithogenic input in marginal basins and deep-sea brines. Deep-Sea Res. Pt II 164, 216-223.

Censi, P., Raso, M., Yechieli, Y., Ginat, H., Saiano, F., Zuddas, P., Brusca, L., D'Alessandro, W., Inguaggiato, C., 2017b. Geochemistry of Zr, Hf, and REE in a wide spectrum of Eh and water composition: the case of Dead Sea Fault system (Israel). Geochem., Geophys., Geosyst. 18, 844-857.

Censi, P., Saiano, F., Zuddas, P., Nicosia, A., Mazzola, S., Raso, M., 2014. Authigenic phase formation and microbial activity control Zr, Hf, and rare earth element distributions in deep-sea brine sediments. Biogeosciences 11, 1125–1136.

Censi, P., Sirota, I., Zuddas, P., Lensky, N., Merli, M., Saiano, F., Piazzese, D., Sposito, F., Venturelli, M., 2020. Trace element fractionation through halite crystallisation. Geochemical mechanisms and environmental implications, Sci. Total Environ. 723, art. 137926

Censi, P., Sposito, F., Inguaggiato, C., Zuddas, P., Inguaggiato, S., Venturi, M., 2018. Zr, Hf and REE distribution in river water under different ionic strength conditions. Sci. Total Environ. 645, 837-853.

Censi, P., Sprovieri, M., Saiano, F., Di Geronimo, S.I., Larocca, D., and Placenti, F. (2007). The behaviour of REEs in Thailand's Mae Klong estuary: Suggestions from the Y/Ho ratios and lanthanide tetrad effects. Estuarine, Coastal and Shelf Science 71(3-4), 569-579.

Chakhmouradian, A.R., Wall, F., 2012. Rare earth elements—Minerals, mines, magnets (and more): Elements 8, 5, 333–340.

Davranche M, Grybos M, Gruau G, Pedrot M, Dia A, Marsac R (2011) Rare earth element patterns: a tool for identifying trace metal sources during wetland soil reduction. Chem Geol 284:127–137

Degens, E.T., Kurtman, F., Eds. The Geology of Lake Van, Min. Res. Explor. Inst. Turkey, Ankara, 1978, pp. 158.

Ekberg, C., Källvenius, G., Albinsson, Y., Brown, P.L., 2004. Studies on the hydrolytic behavior of zirconium (IV). J. Solution Chem. 33, 47-79.

Estrade G., Salvi, S., Béziat, D., Williams-Jones, A.E., 2015. The Origin of Skarn-Hosted Rare-Metal Mineralization in the Ambohimirahavavy Alkaline Complex, Madagascar. Economic Geology, v. 110, pp. 1485–1513.

Firdaus, M.L., Mashio, A.S., Obata, H., McAlister, J.A., Orians, K.J., 2018. Distribution of zirconium, hafnium, niobium and tantalum in the North Atlantic Ocean, north-eastern Indian Ocean and its adjacent seas, Deep-Sea Res. Pt I 140, 128-135.

Firdaus, M.L., Minami, T., Norisuye, K., Sohrin, Y. 2011. Strong elemental fractionation of Zr-Hf and Nb-Ta across the Pacific Ocean. Nat. Geosci. 4, 227–230.

Greaves, M.J., Elderfield, H., Sholkovitz, E.R., 1999. Aeolian sources of rare earth elements to the Western Pacific Ocean. Mar. Chem. 68 (1–2), 31–38.

Grenier, M., Garcia-Solsona, E., Lemaitre, N., Trull, T.W., Bouvier, V., Nonnotte, P., Beek, P., Souhaut, M., Lacan, F., Jeandel, C., 2018. Differentiating lithogenic supplies, water mass transport, and biological processes On and Off the Kerguelen Plateau using rare earth element concentrations and neodymium isotopic compositions. Frontiers in Marine Science, 5 (NOV), art. no. 426.

Haley, B.A., Klinkhammer, G.P., McManus, J., 2004. Rare earth elements in pore waters of marine sediments. Geochim. Cosmochim. Acta 68, 1265–1279. http://dx.doi.org/10.1016/j.gca.2003.09.012.

Hannigan, R. E., Sholkovitz E. R., 2001. The development of middle rare earth element enrichments in freshwaters: Weathering of phosphate minerals, Chem. Geol., 175, 495-508.

Herberling, F., Trainor, T.P., Lützenkirchen, J., Eng, P., Denecke, M.A., Bosbach, D., 2011. Structure and reactivity of the calcite–water interface. J. Coll. Inter. Sci. 354, 843-857.

Inguaggiato, C., Censi, P., Zuddas, P., D'Alessandro, W., Brusca, L., Pecoraino, G., Bellomo, S., 2016. Zirconium-hafnium and rare earth element signatures discriminating the effect of atmospheric fallout from hydrothermal input in volcanic lake water. Chem. Geol. 433, 1–11.

Inguaggiato, C., Censi, P., Zuddas, P., Londono, J.M., Chacon, Z., Alzate, D., Brusca, L., D'Alessandro, W., 2015. Geochemistry of REE, Zr and Hf in a wide range of pH and water composition: the Nevado del Ruiz volcano-hydrothermal system (Colombia). Chem. Geol. 417, 125–133.

Jakubowicz, M., Dopieralska, J., Belka, Z., 2015. Tracing the composition and origin of fluids at an ancient hydrocarbon seep (Hollard Mound, Middle Devonian, Morocco): A Nd, REE and stable isotope study. Geochim. Cosmochim. Acta 156, 50–74.

Jochum, K.P., Seufert, H.M., Spettel, B., Palme, H., 1986. The solar-system abundances of Nb, Ta, and Y, and the relative abundances of refractory lithophile elements in differentiated planetary bodies. Geochim. Cosmochim. Acta 50, 1173-1183.

Johannesson, K.H., Lyons, W.B., 1994. The rare earth element geochemistry of Mono Lake water and the importance of carbonate complexing. Limnology and Oceanography 39 (5), pp. 1141-1154.

Johannesson, K.H., Lyons, W.B., Bird, D.A., 1994. Rare earth element concentrations and speciation in alkaline lakes from the western U.S.A. Geophysical Research Letters 21, 773-776.

Jones, J.V., III, Piatak, N.M., and Bedinger, G.M., 2017, Zirconium and hafnium, chap. V of Schulz, K.J., DeYoung, J.H., Jr., Seal, R.R., II, and Bradley, D.C., eds., Critical mineral resources of the United States—Economic and environmental geology and prospects for future supply: U.S. Geological Survey Professional Paper 1802, p. V1–V26, https://doi.org/10.3133/pp1802V.

Kagi, H., Dohmoto, Y., Takano, S. and Masuda, A., 1993. Tetrad effect in lanthanide partitioning between calcium sulphate crystal and its saturated solution. Chem. Geol. 107, 71-82.

Kerrich, R., Renaut, R.W., Bonli, T., 2002. Trace-element composition of cherts from alkaline lakes in the east African rift: a probe for ancient counterparts. Spec. Publ. 73, 277-298.

Koschinsky, A., Hein, J.R., 2003. Uptake of elements from seawater by ferromanganese crusts: Solid-phase associations and seawater speciation. Mar. Geol. 198, 331-351.

Lee J.H., Byrne R. H. (1993). Complexation of trivalent rare earth elements (Ce, Eu, Gd, Tb, Yb) by carbonate ions. Geochim. Cosmochim. Acta 57, 295-302.

Lemaitre, N., Bayon, G., Ondréas, H., Caprais, J.C., Freslon, N., Bollinger, C., Rouget M. L., De Prunelé A., Ruffine L., Olu-Le Roy K., Sarthou G., 2014. Trace element behaviour at cold seeps and the potential export of dissolved iron to the ocean. Earth Planet. Sci. Lett. 404, 376-388.

Lin, J., Nilges, M.J., Wiens, E., Chen, N., Wang, S., Pan, Y., 2018. Mechanism of Gd^{3+} uptake in gypsum ($CaSO_4 \cdot 2H_2O$): Implications for EPR dating, REE recovery and REE behavior. Geochim. Cosmochim. Acta 258, 63-78.

Liu, X.W., Byrne, R.H., 1998. Comprehensive investigation of yttrium and rare earth element complexation by carbonate ions using ICP-mass spectrometry. J. Solution Chem. 27, 803-815.

Moller, P., Bau, M. 1993. Rare-earth patterns with positive cerium anomaly in alkaline waters from Lake Van, Turkey. Earth Planet. Sci Lett. 117, 671-676.

Möller, P., De Lucia, M., 2020. Incorporation of rare earths and yttrium in calcite: A critical re-evaluation. Aquat. Geochem., 26 (2020), pp. 89-117

Parisi, M. G., Cammarata, I., Cammarata, M., Censi, V., 2017. Rare earths, zirconium and hafnium distribution in coastal areas: The example of Sabella spallanzanii (Gmelin, 1791). Chemosphere 185, 268-276.

Parkhurst, D.L., Appelo, C.A.J., 2010. User's Guide to PHREEQC (Version 2.17.5) - A Computer program for Speciation, Batch- Reaction, One-Dimensional Transport and Inverse Geochemical Calculations. Available at: http://www.brr.cr.usgs.gov/projects/GWC_coupled/phreeqc/index.html.)

Phan, T.T., Hakala, J.A., Lopano, C.L., Sharma S., 2019. Rare earth elements and radiogenic strontium isotopes in carbonate minerals reveal diagenetic influence in shales and limestones in the Appalachian Basin. Chem. Geol. 509, 194-212.

Pinto, H., Haapasilta, V., Lokhandwala, M., Oberg, S., Foster, A.S., 2017. Adsorption and migration of single metal atoms on the calcite (10.4) surface. J. Phys. Condes. Mat. 29, (13)

Playà, E., Cendon, D.I., Trave, A., Chivas, A.R., Garcia, A., 2007. Non-marine evaporites with both inherited marine and continental signatures: The Gulf of Carpentaria, Australia, at similar to 70 ka. Sed. Geol 201, 267-285.

Qu, C.L., Liu, G., Zhao, Y.F., 2009. Experimental study on the fractionation of yttrium from holmium during the coprecipitation with calcium carbonates in seawater solutions. Geochem. J. 43, 403-414.

Raso, M., Censi, P., Saiano, F., 2013. Simultaneous determinations of zirconium, hafnium, yttrium and lanthanides in seawater according to a co-precipitation technique onto iron hydroxide. Talanta 116, 1085–1090.

Reynard, B., Lécuyer, C., Grandjean, P., 1999. Crystal-chemical controls on rare-earth element concentrations in fossil biogenic apatites and implications for paleoenvironmental reconstructions. Chem. Geol. 155, 233-241.

Sillen, L.G., Martell, A.E., 1964. Stability Constants of Metal–Ion Complexes, Special Publication 17, The Chemical Society, London, pp 754.

Taylor, S.R., McLennan, S.M., 1988. The significance of the rare earths in geochemistry and cosmochemistry. Handbook on the Physics and Chemistry of Rare Earths, cap. 79, vol. 11, 485-578.

Taylor, S.R., McLennan, S.M., 1995. The geochemical evolution of the continental crust. Rev. Geophys. 33, 241–265.

Tepe, N., Bau, M., 2015. Distribution of rare earth elements and other high field strength elements in glacial meltwaters and sediments from the western Greenland Ice Sheet: evidence for different sources of particles and nanoparticles. Chem. Geol. 412, 59–68.

Thompson, A., Amistadi, M.K., Chadwick, O.A., Chorover, J. Fractionation of yttrium and holmium during basaltic soil weathering. Geochem. Cosmochim. Acta, 2013, 119, 18-30.

Toulkeridis, T., Podwojewski, P., Clauer, N., 1998. Tracing the source of gypsum in New Caledonian soils by REE contents and S-Sr isotopic compositions. Chem. Geol. 145, 61-71.

Tripathy, S.S., Kanungo, S.B., Mishra, S.K., 2001. The electrical double layer at hydrous manganese dioxide/electrolyte interface. J. Colloid Interface Sci. 241, 112–119.

Wang, J.; Chang, J.; Li, C.; Han, Z.; Wang, T.; Han, H., 2020. Significance of Calcite Trace Elements Contents and C-O Isotopic Compositions for Ore-Forming Fluids and Gold Prospecting in the Zhesang Carlin-Like Gold Deposit of Southeastern Yunnan, China. Minerals 10, 338.

Young, R. The Rietveld Method, International Union of Crystallography, Oxford University Press, Oxford, 1993.

Zhang, L., Algeo, T.J., Cao, L., Zhao, L., Chen, Z. Q., Li, Z., 2016. Diagenetic uptake of rare earth elements by conodont apatite. Palaeogeogr. Palaeoclimatol. Palaeoecol. 458, 176–197.

Zuddas, P., Censi, P., Inguaggiato, C., Sposito, F., 2018 The behaviour of zirconium and hafnium during water-rock interaction. Appl. Geochem. 94, 46–52.

Zuddas, P., Inguaggiato, C., Censi, P., D'Alessandro, W., 2017. Zr-Hf fractionation during water-rock interaction. Procedia Earth and Planetary Science 17, 670–673.

TABLE CAPTIONS

Table 1 - Sampling sites and geographical localisation of studied waters.

Table 2 - Mineralogical composition of studied suspended particulates in lake waters. Values are given in weight %.

FIGURE CAPTIONS

Figure 1 – Geological sketch map of the studied area.

Figure 2 – Major element concentrations analysed in studied waters.

Figure 3 – SEM images of suspended solids in studied water samples filtered with membrane porosity 0.45 µm. Fig. 3a, 3b, 3c, and 3d: Different amounts of build-up in suspended solids mixed to authigenic carbonates in lake waters from different sites. Fig. 3e and 3f: Some particulars of well-developed calcite crystals together with biologic remnants in lake waters. Fig. 3g and 3h: Authigenic solids and lithic fragments are suspended in thermal springs. Fig. 3i: Fine-grained Ca-Mg carbonates and Fe-bearing solids in suspended particles from thermal springs. The open square indicates the area where data to depict X-ray Fluorescence maps of Fe, Ca, and Mg were collected.

Figure 4 – a: Zr and Hf concentration measured in studied water samples and the linear trend depicted by these analyses. b: Zr and Hf concentration measured in suspended solids in studied water samples. c: Zr and Hf concentration measured in halite crystallising from the Dead Sea brine (data from Censi et al., 2020). Measured Zr and Hf concentrations are compared with the range of Zr/Hf values characteristic of crustal rocks and chondrite (Zr/Hf = 71 ± 5.6, Jochum et al., 1986).

Figure 5– Zr/Hf values measured in the dissolved phase of the lake and thermal waters reported towards Ca^{2+} concentration (mol/L) expressed as pCa (see equation 4).

Figure 6 – Shale-normalised REE pattern calculated in the dissolved phase of the lake (a) and thermal waters (b). These features are also depicted in terms of MREE/HREE and LREE/MREE ratios (c). Shale-normalised REE pattern calculated for suspended solids in the lake (d) and thermal waters (e). These features are also reported in terms of MREE/HREE and LREE/MREE ratios (f).

Highlights

- Weathering and authigenic reactions rule the Zr/Hf ratio in natural waters
- Hf shows larger affinity than Zr towards the surface of authigenic calcite
- Calcite crystallisation rules the REE distribution in suspended solids from thermal waters
- Dissolution of airborne particles influences the REE distribution in shallow lake waters

Graphical Abstract

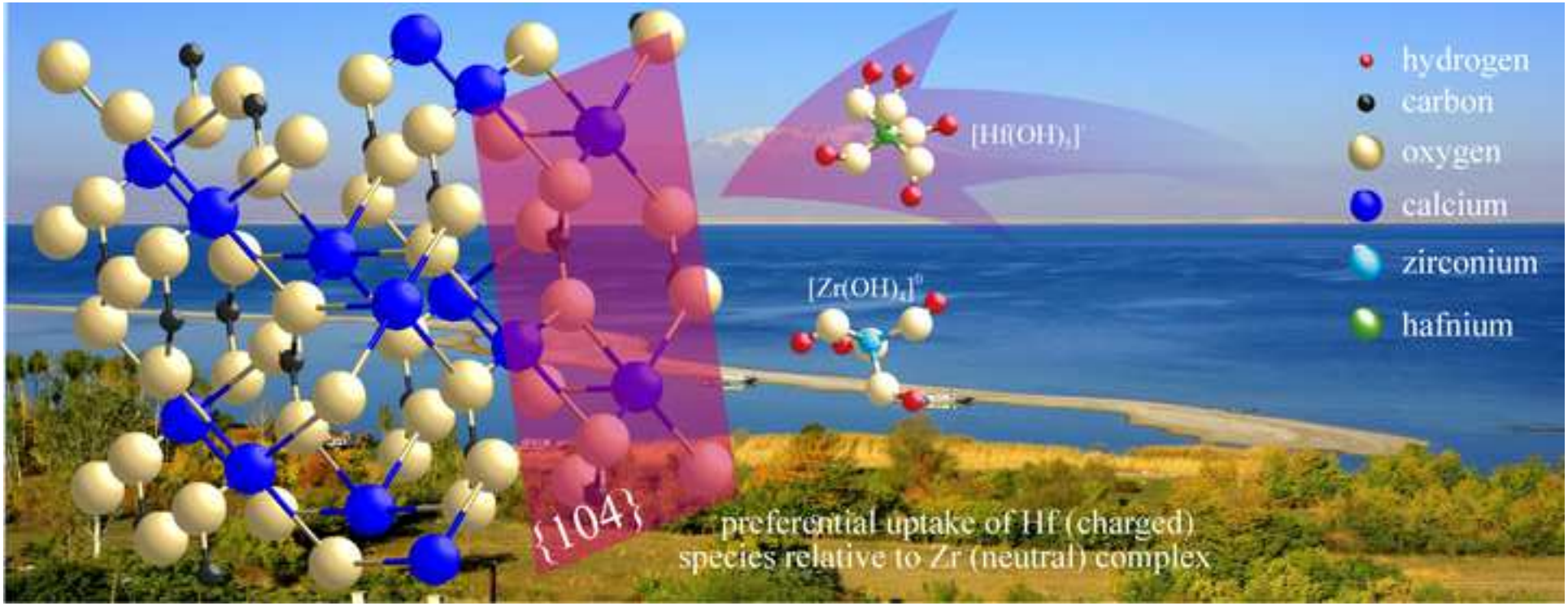

Figure

Click here to access/download;Figure;Fig. 1.jpg

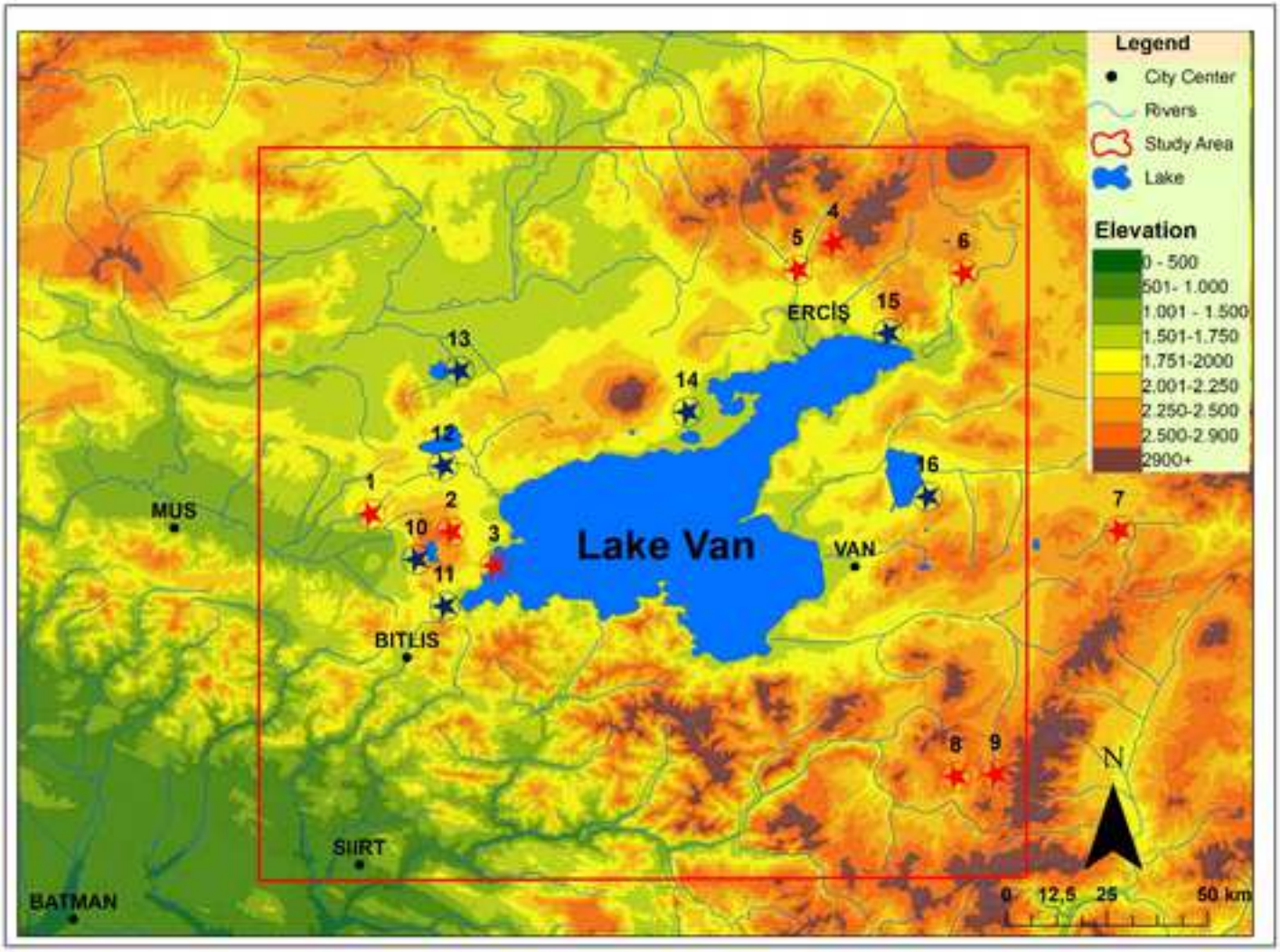

Fig. 1

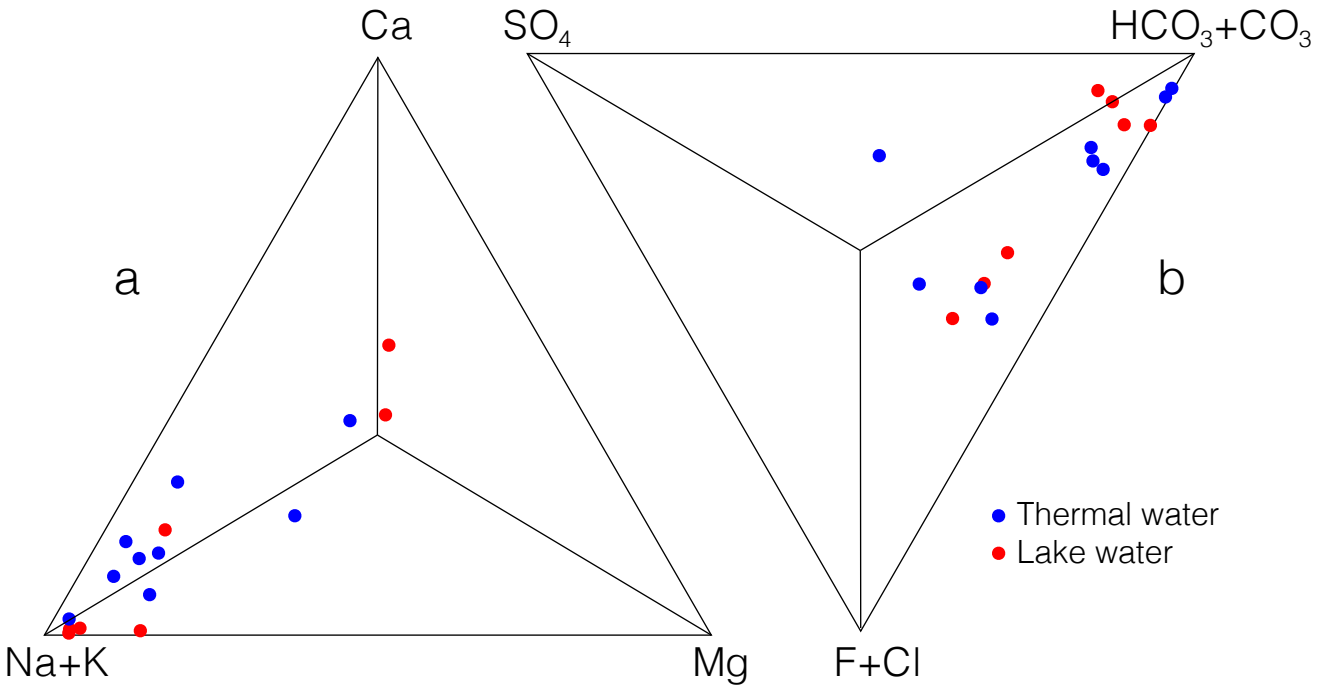

Fig. 2

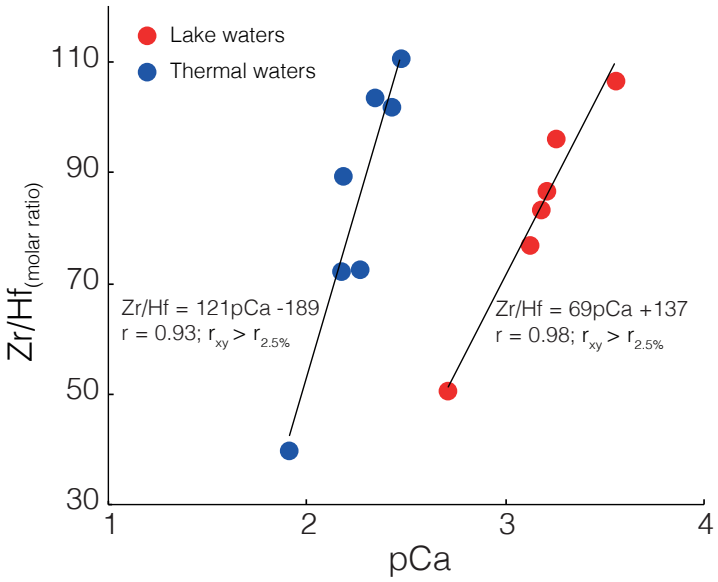

Fig. 5

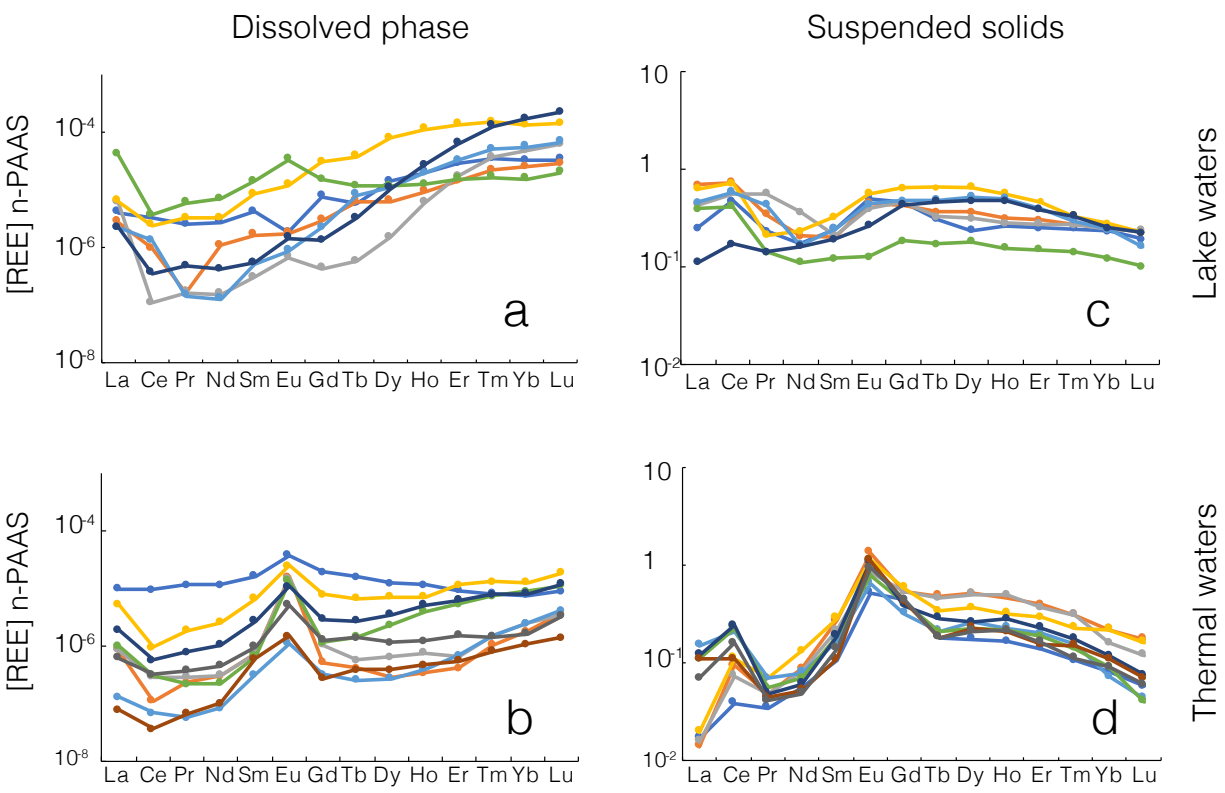

Fig. 6

Figure

Click here to access/download;Figure;Fig. 3.tif

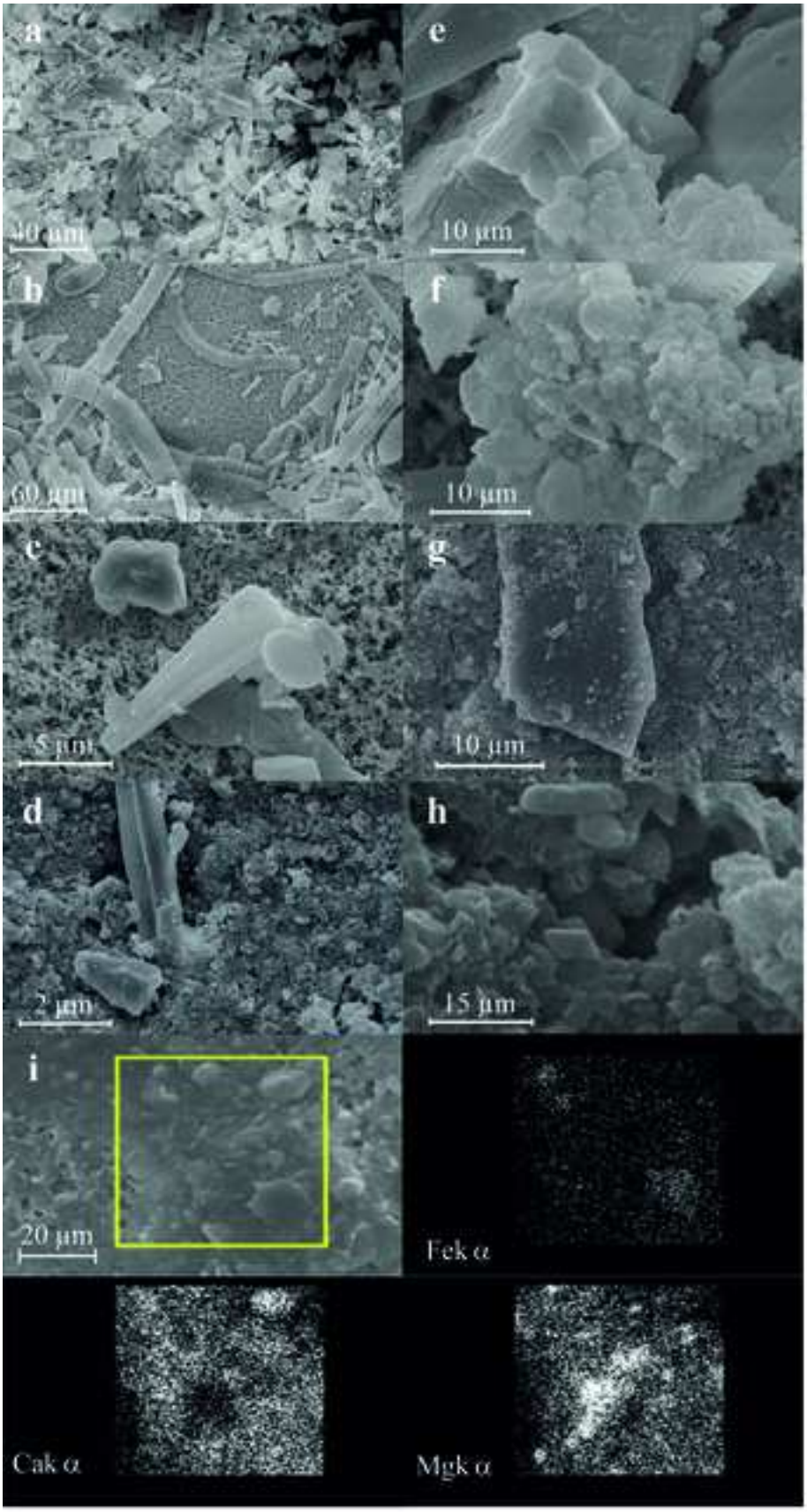

Fig. 3

Figure

Click here to access/download;Figure;Fig. 4.tif

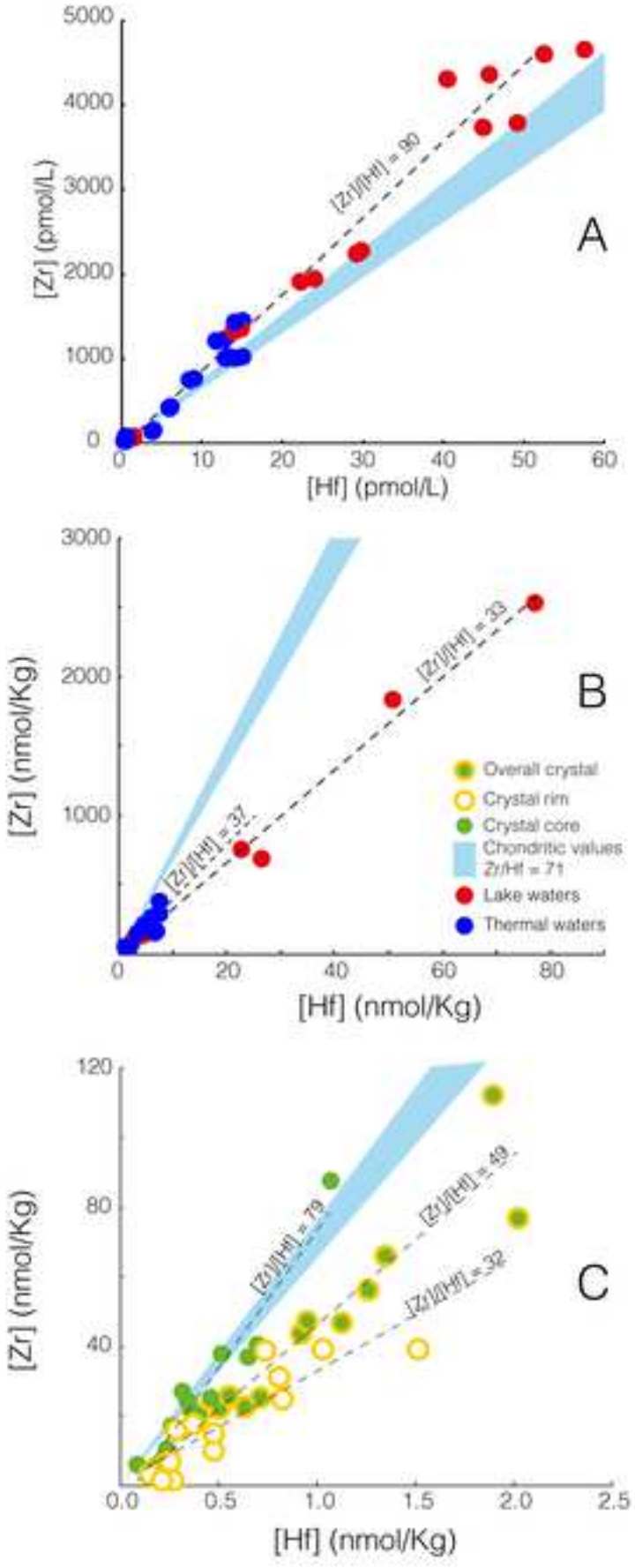

Fig. 4

Table 2

		Mg-calcite	Calcite	Dolomite	Goethite	Quartz
Lake waters	VSL		58	17	13	12
	VEL		35	40	7	15
	VTL		35	46	6	13
	VERL		80	12		8
	VNL		54	35		11
	VHL		68		17	15
	VNML	72	8	13		7

Table 1

Sample number	Location	**Longitude (E)**	**Latitude (N)**	**Altitude (m)**
VSL	Sodali Lake	42.950	38.815	1650
VEL	Van lake Ercis	43.455	38.999	1646
VTL	Van Lake Tatvan	42.336	38.522	1646
VERL	Ercek Lake	43.530	38.647	1803
VNL	Nazik Lake	42.294	38.852	1816
VHL	Hacli Lake	42.314	39.008	972
VNML	Nemrut Lake	42.228	38.623	2247
VSCT	Çaybagi Thermal	44.164	38.517	2070
VBDT	Dereici (Baskale) Thermal	43.951	37.838	2260
VBZT	Zereni (Baskale) Thermal	44.089	37.798	2180
VEHT	Hasan Apdal (Ercis) Thermal	43.388	39.225	1890
VGT	Gülsuhan (Tatvan) Thermal	42.394	38.591	1648
VCT	Caldiran Thermal	43.863	39.120	2050
VGCT	Cukur (Guroymak) Thermal	42.027	38.655	1480
VNMT	Nemrut Thermal	42.246	38.625	2250
VETT	Taskapi (Ercis) Thermal	43.430	39.270	1930

UNIVERSITÀ DEGLI STUDI DI PALERMO

Dipartimento di Scienze della Terra e del Mare (DiSTeM)

COD. FISC. 80023730825 ~ P.IVA 00605880822

Palermo, November 14, 2020

CONFLICT OF INTEREST DECLARATION

I subscribed Prof. Paolo Censi, as corresponding author of the paper: "*Zirconium and Hafnium fractionation and distribution of Rare Earth Elements in neutral-alkaline waters: Case study of Lake Van hydrothermal system, Turkey*"

DECLARE

that do not occur conflicts of interest in the submission of the above mentioned paper to *Journal of Geochemical Exploration.*

UNIVERSITÀ DEGLI STUDI DI PALERMO

Dipartimento di Scienze della Terra e del Mare (DiSTeM)

COD. FISC. 80023730825 ~ P.IVA 00605880822

Palermo, March 8th, 2021

All the authors contribute to the same extent to the study leading to the submission of the manuscript entitled "Zirconium and hafnium fractionation and distribution of Rare Earth Elements in neutral–alkaline waters: Case study of Lake Van hydrothermal system, Turkey"

Sincerely yours,

Paolo Censi

Dr. Paolo Censi
Professor (Geochemistry)
University of Palermo
Department of Earth and Marine Sciences
Via Archirafi, 36 - 90123 PALERMO (Italy)
Phone: +3909123861639
e-mail: paolo.censi@unipa.it

Zirconium and hafnium fractionation and distribution of Rare Earth Elements in neutral–alkaline waters: Case study of Lake Van hydrothermal system, Turkey

Sasmaz A.[1], Zuddas P.[2], Cangemi M.[3], Piazzese D.[3], Ozek G.[1], Venturi M.[4], Censi P.[3*]

1. Firat University, Geological Engineering, 23119, Elazig (Turkey)
2. Sorbonne Université, CNRS, METIS - 4, Rue Jussieu, F75005, Paris (France)
3. University of Palermo, DiSTeM, Via Archirafi 22, 90123, Palermo (Italy)
4. SIDERCEM S.R.L., Via Libero Grassi 7, 93100 Caltanissetta (Italy).

• corresponding author paolo.censi@unipa.it +393479662844

Abstract

We investigated the distribution of Zr, Hf, and rare earth elements (REE) as the sum of lanthanides plus Y) in the hydrothermal system in the Lake Van area of south-eastern Turkey. This system is characterised by water with variable pH in alkaline conditions resulting from hydrothermal CO_2 upraise and neoformation of calcite minerals in near equilibrium with the interacting waters. Zr, Hf, and REE determinations were carried out for aqueous phases and suspended solids in lake water and surrounding thermal springs. We found that dissolved Hf is partitioned relative to Zr during calcite formation and that such fractionation is a function of the Ca^{2+} activity in warm water. The observed Zr-Hf fractionation is explained by coulombic interactions that occur between suspended solid particles and dissolved phases at the calcite-water interface. There, the surfaces of carbonate minerals demonstrated greater reactivity towards aqueous Hf-bearing species relative to Zr-complexes. This evidence involves a coulombic mechanism of reactivity at the calcite-water interface because Hf complexes are negatively charged while Zr compounds are uncharged. Thus,

26 authigenic calcite can behave as a suitable host for dissolved metal ion species to adsorb on crystal
27 surfaces to remediate waste waters from mine drainage.
28
29 Keywords
30 Zr/Hf ratio; REE; Alkaline lakes; Turkey

1 Introduction

Zirconium, Hf, and rare-earth elements (REE) are used in specialised technology industries notwithstanding their limited production (Chakhmouradian and Wall, 2012; Jones III et al., 2017). Demand for these elements is high leading an effort by the mineral exploration industry to understand genetic processes and discover new resources. Geochemically, these elements were considered to be 'immobile' in subsurface conditions while some works indicate easy water transport under subsurface hydrothermal conditions (Michard and Albarede, 1986; Michard, 1989). Accordingly, REE enrichment has been observed in deposits formed from carbonisation in alkaline environments where Zr concentrations were enriched by a factor of 3 to 4 (Estrade et al., 2015). The behaviour of these strategic elements under surface and subsurface conditions is often neglected because of difficulties in accurate analytical determination at the level of pmol/kg in natural water. In a recent survey, the dissolved Zr/Hf ratio was different from that found in the rock minerals (Censi et al., 2020; Cidu et al., 2013; Inguaggiato et al., 2015, 2016; Parisi et al., 2017; Tepe and Bau, 2015; Zuddas et al., 2017, 2018) suggesting that the subsurface cycle is important in the accumulation of these elements. In fact, the Zr/Hf molar value in rock minerals was 71±6 which corresponds to the so-called 'chondritic' signature (Jochum et al., 1986), while natural water had a wider range of Zr/Hf (Zuddas et al., 2018). The supergene geochemical cycle of Zr and Hf participates in the accumulation and stability of these elements through the process of dissolution and precipitation of the minerals. Because the composition of subsurface and surface waters is often near equilibrium with carbonate minerals like calcite, calcite is expected to play a significant role in the supergene behaviour of these elements. Although carbonates are among the most common minerals in equilibrium with natural water, the formation of neogenic calcite also determined the change in REE distribution observed by Moller and De Lucia (2020) in controlled laboratory investigations. To explain Zr-Hf decoupling during calcite crystallisation and the concurrent behaviour of REEs, we investigated the distribution of these elements in a natural hydrothermal system characterised by the formation of calcite under the neutral and alkaline water system found at

Lake Van and characterised by low thermal and lake waters with pH ranging from 6 to 10, resulting from a variable CO_2 flux (Degens and Kurtman, 1978; Moller and Bau, 1993). The Lake Van system is characterised by neogenic precipitation in the form of Ca-Mg carbonates (Moller and Bau, 1993).

2 Material and Methods

Lake Van is located in south-eastern Turkey (Fig. 1) which formed during the collision between European and Arabian plates. The sequence starts with Paleozoic metamorphic rocks overlaid by Permian limestones and schists followed by sediments of marine and continental origin (Upper Cretaceous-Pliocene) closed by basic and felsic volcanic-pyroclastic rocks (Oligocene-Recent) (Degens and Kurtman, 1978, Yilmaz, 1990). Heat flow data suggest the presence of a magmatic body beneath the lake bottom, possibly related to Nemrut Volcano and sustaining input of CO_2 into Lake Van waters (Moller and Bau, 1993). Presently, the Lake Van represents the largest soda lake worldwide resulting from a combined volcanogenic hydrothermal CO_2 input and seasonal evaporitic conditions (Moller and Bau, 1993).

2.1 Field sampling

Field study and water sampling were conducted in November 2018 and consisted of 16 samples collected from lake water and thermal springs. Coordinates and geologic units of the collected samples are given in Table 1. Lake water was sampled at a depth of 15–20 cm. Physicochemical parameters (pH, redox potential (Eh), temperature, and electrical conductivity) were measured with an Eh oxytrode Pt probe (Hamilton^{TM}) using a standard reference solution buffer at 0.475±0.005 V. Accuracy of determinations was ±10 mV. For the major ion determinations, water samples were filtered in the field through 0.45 μm Millipore® cellulose acetate filters into 50 mL polyethylene bottles and acidified with ultrapure HNO_3. Water samples for trace and rare element analyses were collected in 2,000 mL Nalgene bottles at each sampling site.

2.2 Water analysis and thermodynamic modelling

In the laboratory, samples were filtered (Millipore® manifold filter, 47 mm diameter with a 0.45 μm pore size cellulose nitrate membrane), then 5% ultrapure HNO_3 acid solution was added to

reach pH ≈ 2. Zirconium, Hf, and REEs in aqueous samples were analysed according to the methods of Raso et al. (2013). Briefly, an excess of $FeCl_3$ (1%) solution was added to each sample (1 L), and a suitable volume of NH_4OH (25%) solution was added to attain a pH of 8 to induce precipitation of solid $Fe(OH)_3$. During this process, Zr, Hf, and REEs were held onto the surface of the crystallising solid. To ensure that crystallisation of $Fe(OH)_3$ was complete, the solution was left in a closed flask for 48–72 h in a stirrer. Next, the iron concentration was measured to assess recovery and was consistently greater than 95%. Precipitated $Fe(OH)_3$, together with Zr, Hf, and REEs, was collected on a membrane filter (Millipore® manifold filter, 47 mm diameter with 0.45 μm pore size). The solid filtrate was then dissolved in 3 M HCl, and the obtained solution was diluted to 1 M HCl prior to analysis using a Quadrupole-ICP-MS (Agilent 7800 series) with an external calibration procedure. The overall strategy and a detailed evaluation of the analytical errors were reported in Raso et al. (2013). The overall enrichment factor measured for Zr, Hf, and REE concentrations corresponded to 66.7.

Lanthanum, Ce, and Eu anomalies were calculated using equations 1–3 (Alibo and Nozaki, 1999):

$$\frac{La}{La^*} = \frac{[La]_n}{3*[Pr]_n+2*[Nd]_n}, \quad (1)$$

$$\frac{Ce}{Ce^*} = \frac{2*[Ce]_n}{[La]_n+[Pr]_n}, \text{ and} \quad (2)$$

$$\frac{Eu}{Eu^*} = \frac{2*[Eu]_n}{[Sm]_n+[Gd]_n}, \quad (3)$$

where the subscript n indicates shale-normalised elemental concentrations calculated relative to the Post Archean Australian Shale (PAAS, Taylor and McLennan, 1995).

All chemicals used during laboratory manipulations were ultrapure grade. Ultrapure water (resistivity of 18.2 MΩ cm or better) was obtained from an Arium® mini system (Sartorius, Italy). HNO_3 65%, NH_4OH (20%) and HCl (30%) solutions were purchased from J.T. Baker (ULTREX II) chemicals. Working standard solutions of the elements studied were prepared daily by stepwise dilution of standard multi-element stock solutions from DBH, Merck, or CPI International (1,000±5

mg/L) in a 1 M HCl medium. All labware was polyethene, polypropylene, or Teflon® and the calibration of all volumetric equipment was verified. Assessment of the analytical precision of Zr, Hf, and REEs was performed on five aliquots (500 mL each) of NASS-6 (seawater certified reference material for trace metals) distributed by the National Research Council of Canada. These certified reference materials were treated as water samples according to the procedure mentioned above and the concentrations obtained were compared with those previously reported by Raso et al. (2013) and Lemaitre et al. (2014). Analysed values are reported in Supplementary Data 1.

Thermodynamic modelling of the chemical composition of the water performed was using PHREEQC software and adding additional Lawrence Livermore National Laboratory (LLNL) database (version 3.0.6, Parkhurst and Appelo, 2010).

2.3 Suspended solids

X-ray diffraction investigations were carried out with a Philips PW14 1373 X-ray spectrometer (Cu-Kα radiation 2Θ range 10–40°, step size 0.02°, and a 1-min step time). The X-ray spectra were analysed by the Rietveld method (Program DiffracPlus TOPAS®, Version 4.0, Bruker AXS Inc., Karlsruhe, Germany) using parameters for the Rietveld refinement method obtained from the Inorganic Crystal Structure Database (ICSD) program. This method consists of fitting the experimental XRD spectrum to the theoretical spectrum (Young, 1993). A detailed explanation of the method is reported in Scarlett and Madsen (2006).

Scanning electron microscopy (SEM) of suspended particles was carried out on materials collected after filtration onto cellulose nitrate membranes. Dried solids were mounted on an aluminium stub and gold coated. The SEM analyses were carried out using a LEO 440 SEM equipped with an EDS system OXFORD ISIS Link and Si (Li) PENTAFET detector at the SIDERCEM SRL laboratory (Caltanissetta, Italy). Chemical analyses were carried out by digesting 100 mg of each sample in 10 mL of a 1:1 HNO_3:H_2O_2 mixture in a sealed Teflon® TFM bomb using a microwave oven (CEM MARS 5 device). After digestion, the TFM bomb was rinsed, and the solution was filtered onto

previously acid-cleaned 0.45 μm Millipore® filters to remove silicate residue. The filtered solution was diluted to 50 mL and stored for chemical analyses.

3 Results and Discussion

3.1 System description

The concentration of major elements, pH, Eh, electric conductivity, and temperature are reported in the Supplementary Data 2. Water samples had ionic strength ranging from 0.024 to 0.222 M in thermal water and between 0.004 and 0.443 M in lake water. Thermal water had pH between 5.8 and 7.1 and Eh between 0.01 and 0.17 V, while lake water had pH between 8 and 10 and Eh from -0.29 and 0.01 V. Figure 2a shows that lake water preferentially falls in the field of alkaline elements (only two samples have higher Ca^{2+} and Mg^{2+}concentrations) while thermal water fell between alkaline and Ca^{2+}-rich field (few samples fell in the Mg^{2+} corner).

The SEM images of the suspended particulates revealed that suspended particulate matter in lake water consisted of authigenic carbonates associated with biogenic detritus and lithic fragments (Fig. 3a-f), while suspended solids in thermal waters were authigenic carbonates and Fe-rich particles and lithogenic fragments (Fig. 3g-i). Iron-bearing particulates in the samples were often mixed with authigenic calcite and dolomite (see elemental maps in Fig. 3i). The X-ray diffraction analyses confirmed the presence of carbonate minerals identified as calcite and low-Mg calcite representing up to 80% of the authigenic minerals (Table 2). Other phases collected were Fe-oxyhydroxides and detritic silicate particles reaching 10–15% of the total mass.

Using the chemical composition of the collected samples, we estimated the saturation state with respect to the mineral in equilibrium and found both lake water and thermal water were saturated or oversaturated with respect to calcite or low-Mg calcite. Some water was also saturated with respect to dolomite and goethite in agreement with the results of the X-ray determinations of the collected suspended matter.

3.2 Zr and Hf behaviour

Zr and Hf concentrations in both aqueous and suspended particulate matter are reported in Supplementary Data 3 and 4, respectively. In the aqueous phase, the concentration of Zr and Hf was not homogenous. Lake waters had Zr concentrations between 79 and 4958 pmol/L while Hf concentrations fell between 2 and 53 pmol/L, and thermal waters had Zr concentrations between 32 and 1.4 pmol/L; whereas Hf concentrations fell between 0.5 and 14 pmol/L. The concentrations of Zr and Hf in thermal waters were 1 to 3 orders of magnitude lower than those found in lake water; however, the concentration of Zr as a function of Hf was linearly correlated with an intercept equal to zero and parametrising a single slope of 90±2 (Fig. 4a). This value was higher than the Zr/Hf value of 71±6 for crustal materials and chondrites (Jochum et al., 1986) indicating that the calcite precipitation fractionates the Zr/Hf ratio in water. In the suspended solids from lake water, Zr concentration ranged from 99 to 2533 nmol/kg, whereas Hf fell between 2.6 and 77.1 nmol/kg. Suspended solids from thermal water had Zr concentrations between 20.7 and 346.7 nmol/kg and Hf between 0.6 and 6.8 nmol/kg. Similarly, Zr and Hf in solids collected from thermal water were lower compared to suspended solids found in lake water. Figure 4B shows the concentration of Zr as a function of Hf in neogenic calcite from lake water and describes a linear slope of 33.5 similar to calcite in equilibrium with thermal water where the slope was 37.

These results show that the Zr/Hf ratio in water is different from that in crustal rocks and that Hf is preferentially enriched in authigenic carbonate minerals. Preferential enrichment of Hf relative to Zr in newly-formed suspended carbonates was unexpected and may result from processes occurring at the surface-water interface. The calcite-water interface is generally represented by an electric double-layer of weak mineral solubility buffered by CO_3^{2-} ions with the ζ potential of the {104} carbonate surface independent of pH (Herberling et al., 2011). Laboratory measurements indicate the positive surface potential (up to 24 mV) when the Ca^{2+} concentration in solution is between 10^{-2} and 10^{-4} M (Al-Mahrouqui et al., 2017). Byrne (2002) made a critical review of stability constants for Zr and Hf hydroxyl complexes based on the work of Sillen and Martell (1964), Baes and Mesmer (1976), Ekberg et al. (2004), and Brown et al. (2005) and estimated that the most

abundant Zr and Hf complexes in aqueous phase were $[Zr(OH)_4]^0$ and $[Hf(OH)_5]^-$, respectively (Koschinsky and Hein, 2003). Reporting Zr/Hf ratios as a function of pCa:

$$pCa = -Log(a_{Ca^{2+}}) (4)$$

(Fig. 5), we found two distinct correlation lines, one for thermal water and one for lake water, suggesting that negatively-charged $[Hf(OH)_5]^-$ complexes were preferentially scavenged onto {104} positive carbonate surfaces and were, in turn, removed from the aqueous phase. This potential mechanism explains the Zr/Hf fractionation observed during calcite precipitation under pH conditions between 7 and 10 and should correspond to the higher binding energy between Hf and {104} calcite surface relative to Zr as estimated by theoretical ab initio calculations (Pinto et al., 2017). Our results support the Zr/Hf fractionation observed by Firdaus et al. (2011, 2018) during Fe-oxyhydroxide formation. Fe-oxyhydroxide was in fact positively charged under weak alkaline conditions (Koschinsky and Hein, 2003). On the contrary, Zr-Hf fractionation did not occur onto surfaces of Mn-oxyhydroxides that were negatively charged at the pH up to acidic values (Tripathy et al., 2001). The Zr-Hf fractionation here observed during calcite formation and interpreted as water-interface interaction is consistent with the Zr-Hf fractionation found in stromatolites (Censi et al., 2015), halite (Censi et al., 2017a, 2020), and other groundwater environments (Censi et al., 2017b; Inguaggiato et al., 2015, 2016).

3.3 REE behaviour

Dissolved REE concentrations in lake water and thermal water in the Lake Van system ranged between 7135 and 76140 pmol/L and from 168 to 17426 pmol/L, respectively (Supplementary Data 3). In lake waters the shale normalised pattern (Fig. 6a) reveals the presence of La positive anomaly as well an 'ascending' feature leading to enrichment in heavy REE (HREE, from Ho to Lu) while thermal waters have a single slight medium REE (MREE, from Sm to Dy) enrichment (Fig. 6b). In both types of water, Eu anomalies were 0.3 and 4.8 without evidence of a positive Ce anomaly ($0.1 \leq Ce/Ce^* \leq 1$). The progressive increase of REEs observed in the normalised patters in these waters may result from the values of the stability constants of di-

carbonate and carbonate REE-complex ions (Lee and Byrne, 1993; Liu and Byrne, 1998) potentially producing $[REE(CO_3)_2]^-$ complexes (Johannesson et al., 1994; Johannesson and Lyon, 1994; Kerrich et al., 2002; Moller and Bau, 1993). Our data showed a higher abundance of La and therefore inconsistent with earlier REE measurements from Van Lake waters (Moller and Bau, 1993). The water level of Lake Van has dropped due to climate change over the last 30 years while the input of lithogenic solids increased. The main difference between the REE distribution recognised in lake Van waters and that reported by Moller and Bau (1993) is the lack of positive Ce anomaly in our samples. This may be caused by a larger dissolution of lithogenic particles typical of continental and coastal waters. The dissolution of lithogenic solids usually provides La enrichment in the aqueous phase that can conceal the concurrent Ce enrichment completely or partially (Censi et al., 2007; Greaves et al., 1999; Grenier et al., 2018).

Suspended particulate material collected from the lake and thermal waters had a total concentration of REEs ranging between 508.2 and 835.2 nmol/kg and from 102.3 to 278.5 nmol/kg, respectively (Supplementary Data 4). These values are 3 to 4 orders of magnitude higher than the concentrations found in related waters. The shale-normalised REE patterns of suspended calcites collected in lake waters (Fig. 6c) and thermal waters (Fig. 6d) display positive Ce anomalies ranging from 1.1 to 3.1, an enrichment in MREEs with positive Eu anomalies ($0.8 < Eu/Eu^* < 4.2$), and slight progressive depletion of HREEs. Suspended solids from thermal waters showed ‘bulged’ REE patterns (Fig. 6d) while solids from lake waters had flatter patterns (Fig. 6C). The REE distribution in shale-normalised patterns usually show MREE enrichment mainly ruled by crystal-chemical reasons, as demonstrated by the review of distribution coefficient values reported by Moller and De Lucia (2020). In suspended solids from thermal water, the MREE enrichment was more evident than in materials collected from lake water. This evidence is probably justified by the concurrent presence of a detrital fraction in the ‘bulge’ of suspended solids from lake water with a ‘flatter’ shale-like trend in the normalised concentration (Taylor and McLennan, 1988).

The behaviour of Y-Ho twin is different in lake and thermal waters. In lakes, Y and Ho concentrations ranged from 3845 to 62279 pmol/L and 36 to 686 pmol/L respectively, whereas in thermal springs, Y ranges up to 3577 pmol/L, whereas Ho fell between 2 and 68 pmol/L. The related Y/Ho ratios spanned from 51 to 111 in lake water and between 53 and 162 in thermal water. These ratios fell between chondritic and super-chondritic values. On the contrary, in carbonates from suspended solids, the Y/Ho ratio ranged from 32.4 to 49.6 in lake water and from 28.6 and 47.8 in thermal water. Then Y/Ho values in suspended solids spanned between slight subchondritic to chondritic values (Y/Ho = 52±5, Jochum et al., 1986).

The role played by the formation of calcite in the distribution of REEs in alkaline waters was highlighted by the super-chondritic value of the Y/Ho ratio. Our study revealed that Ho was 2 to 3 orders of magnitude higher than Y during calcite formation causing enrichment. The preferential enrichment of Ho in calcite compared to Y observed in our study may reflect the larger value of the Misono softness parameter of Ho^{3+} relative to Y^{3+} (Thompson et al., 2013) due to the different external electronic configuration of these metal ions (Qu et al., 2009).

The different fractionation of these elements found during the formation of calcite also reflects other processes. In thermal water, the intensity of the water-rock interaction may cause MREE enrichment (Fig. 6c). Dissolution of lithogenic rocks may be the source of MREE (Bau, 1999; Censi et al., 2019; Greaves et al., 1999; Haley et al., 2004; Inguaggiato et al., 2016; Lin et al. 2019) and explain MREE enrichment observed in authigenic hydrothermal carbonates (Jakubowicz et al., 2015; Phan et al., 2019; Wang et al., 2020), phosphates (Censi et al., 2007; Hannigan and Sholkovitz, 2001; Reynard et al., 1999; Zhang et al., 2016), sulphates (Censi et al., 2014; 2018; Kagi et al., 1993; Playà et al., 2007; Toulkeridis et al., 1998), and Fe-oxyhydroxides (Bau, 1999; Davranche et al., 2011).

4 Implications and Conclusions

The results of our investigation of water oversaturated with calcite indicate that calcite plays a crucial role in constraining Zr-Hf fractionation and the geochemical behaviour of REEs in alkaline

lake waters. The strong reactivity of positively charged {104} surfaces of calcite coupled with the aqueous Zr and Hf speciation lead to preferential accumulation of Hf in calcite relative to Zr. This indication agrees with the larger affinity of Hf towards solid surfaces relative to Zr already evidenced onto the surfaces of Fe-oxyhydroxides. But the Hf removal onto the carbonate surfaces is ruled by pCa, whereas onto the Fe-oxyhydroxide surfaces is ruled by pH. Therefore, changes of the Zr/Hf ratio in natural waters relative to the chondritic signature indicate that these elements are involved in processes occurring at the interface with crystallising authigenic minerals.

Differences in the external electronic configuration of Zr and Hf is similar to that between Y and Ho due to differences in softness/hardness between Zr and Hf and between Y and Ho that, in turn, influence hydrolysis during formation of Zr and Hf hydroxyl complexes. This process could be a crucial aspect of the fractionation of these metal ions during calcite formation. Differences in softness between Y and Ho lead increase stability of Ho-O relative to Y-O bonds on solid surfaces and rule Y-Ho fractionation at the solid-liquid interface.

Based on previous researches addressed to the larger Hf affinity relative to Zr towards crystal surfaces of halite, potash salts and Fe-oxyhydroxides, this study contributes to demonstrate that the larger surface reactivity of Hf relative to Zr is a widespread phenomenon through the sedimentary processes. The evidence of this phenomenon is detected measuring the Zr/Hf ratio in natural waters and in authigenic minerals.

ACKNOWLEDGMENT

This research was partially funded by the contracts CORI 2017 (University of Palermo) and CON-0037 funded by the SIDERCEM S.R.L. - University of Palermo Agreement and The Science and Technological Research Council of Turkey (TUBITAK 118Y319).

285 REFERENCES

286 Al-Mahrouqi, D.A., Vinogradov, J., Jackson, M.D., 2017. Zeta potential of artificial and natural
287 calcite in aqueous solution. Adv. Colloid. Interface Sci. 240, 60-76.
288 Alibo, D.S., Nozaki, Y., 1999. Rare earth elements in seawater: Particle association, shale-
289 normalization, and Ce oxidation. Geochim. Cosmochim. Acta 63, 363-372.
290 Baes, C. F., Mesmer R. S. 1976. The Hydrolysis of Cations. John Wiley & Sons, Ltd, New York,
291 London, Sydney, Toronto.
292 Bau, M., 1999. Scavenging of dissolved yttrium and rare earths by precipitating iron oxyhydroxide:
293 Experimental evidence for Ce oxidation, Y-Ho fractionation, and lanthanide tetrad effect.
294 Geochim. Cosmochim. Acta 63, 67–77.
295 Brown, P.L., Curti, E., Grambow, B. Chemical Thermodynamics of Zirconium, Mompean J. P.,
296 Perrone J. (eds.) NEA Data Bank, OECD 2005, pp 512.
297 Byrne, R.H., 2002. Inorganic speciation of dissolved elements in seawater: The influence of pH on
298 concentration ratios. Geochem. T. 3, 11-16.
299 Censi, P., Cangemi, M., Brusca, L., Madonia, P., Saiano, F., Zuddas, P., 2015. The behaviour of
300 rare-earth elements, Zr and Hf during biologically-mediated deposition of silica-stromatolites and
301 carbonate-rich microbial mats. Gondwana Res. 27, 209-215.
302 Censi, P., Inguaggiato, C., Chiavetta, S., Schembri, C., Sposito, F., Censi, V. and Zuddas, P. (2017a)
303 The behaviour of zirconium, hafnium and rare earth elements during the crystallisation of halite
304 and other salt minerals. Chem Geol 453, 80-91.
305 Censi, P., Raso, M., Saiano, F., Zuddas, P., Oliveri, E., 2019. Zr/Hf ratio and REE behaviour: A
306 coupled indication of lithogenic input in marginal basins and deep-sea brines. Deep-Sea Res. Pt II
307 164, 216-223.
308 Censi, P., Raso, M., Yechieli, Y., Ginat, H., Saiano, F., Zuddas, P., Brusca, L., D'Alessandro, W.,
309 Inguaggiato, C., 2017b. Geochemistry of Zr, Hf, and REE in a wide spectrum of Eh and water

composition: the case of Dead Sea Fault system (Israel). Geochem., Geophys., Geosyst. 18, 844-857.

Censi, P., Saiano, F., Zuddas, P., Nicosia, A., Mazzola, S., Raso, M., 2014. Authigenic phase formation and microbial activity control Zr, Hf, and rare earth element distributions in deep-sea brine sediments. Biogeosciences 11, 1125–1136.

Censi, P., Sirota, I., Zuddas, P., Lensky, N., Merli, M., Saiano, F., Piazzese, D., Sposito, F., Venturelli, M., 2020. Trace element fractionation through halite crystallisation. Geochemical mechanisms and environmental implications, Sci. Total Environ. 723, art. 137926

Censi, P., Sposito, F., Inguaggiato, C., Zuddas, P., Inguaggiato, S., Venturi, M., 2018. Zr, Hf and REE distribution in river water under different ionic strength conditions. Sci. Total Environ. 645, 837-853.

Censi, P., Sprovieri, M., Saiano, F., Di Geronimo, S.I., Larocca, D., and Placenti, F. (2007). The behaviour of REEs in Thailand's Mae Klong estuary: Suggestions from the Y/Ho ratios and lanthanide tetrad effects. Estuarine, Coastal and Shelf Science 71(3-4), 569-579.

Chakhmouradian, A.R., Wall, F., 2012. Rare earth elements—Minerals, mines, magnets (and more): Elements 8, 5, 333–340.

Cidu R., Vittori Antisari L., Biddau R., Buscaroli A., Carbone S., Da Pelo S., Dinelli E., Vianello G., Zannoni D., 2013. Dynamics of rare earth elements in water-soil systems: the case study of the Pineta San Vitale (Ravenna, Italy). Geoderma 193-194: 52-67.

Davranche M, Grybos M, Gruau G, Pedrot M, Dia A, Marsac R (2011) Rare earth element patterns: a tool for identifying trace metal sources during wetland soil reduction. Chem Geol 284:127–137

Degens, E.T., Kurtman, F., Eds. The Geology of Lake Van, Min. Res. Explor. Inst. Turkey, Ankara, 1978, pp. 158.

Ekberg, C., Källvenius, G., Albinsson, Y., Brown, P.L., 2004. Studies on the hydrolytic behavior of zirconium (IV). J. Solution Chem. 33, 47-79.

335 Estrade G., Salvi, S., Béziat, D., Williams-Jones, A.E., 2015. The Origin of Skarn-Hosted Rare-
336 Metal Mineralization in the Ambohimirahavavy Alkaline Complex, Madagascar. Economic
337 Geology, v. 110, pp. 1485–1513.
338 Firdaus, M.L., Mashio, A.S., Obata, H., McAlister, J.A., Orians, K.J., 2018. Distribution of
339 zirconium, hafnium, niobium and tantalum in the North Atlantic Ocean, north-eastern Indian
340 Ocean and its adjacent seas, Deep-Sea Res. Pt I 140, 128-135.
341 Firdaus, M.L., Minami, T., Norisuye, K., Sohrin, Y. 2011. Strong elemental fractionation of Zr-Hf
342 and Nb-Ta across the Pacific Ocean. Nat. Geosci. 4, 227–230.
343 Greaves, M.J., Elderfield, H., Sholkovitz, E.R., 1999. Aeolian sources of rare earth elements to the
344 Western Pacific Ocean. Mar. Chem. 68 (1–2), 31–38.
345 Grenier, M., Garcia-Solsona, E., Lemaitre, N., Trull, T.W., Bouvier, V., Nonnotte, P., Beek, P.,
346 Souhaut, M., Lacan, F., Jeandel, C., 2018. Differentiating lithogenic supplies, water mass
347 transport, and biological processes On and Off the Kerguelen Plateau using rare earth element
348 concentrations and neodymium isotopic compositions. Frontiers in Marine Science, 5 (NOV), art.
349 no. 426.
350 Haley, B.A., Klinkhammer, G.P., McManus, J., 2004. Rare earth elements in pore waters of marine
351 sediments. Geochim. Cosmochim. Acta 68, 1265–1279. http://dx.doi.org/10.
352 1016/j.gca.2003.09.012.
353 Hannigan, R. E., Sholkovitz E. R., 2001. The development of middle rare earth element enrichments
354 in freshwaters: Weathering of phosphate minerals, Chem. Geol., 175, 495-508.
355 Herberling, F., Trainor, T.P., Lützenkirchen, J., Eng, P., Deneke, M.A., Bosbach, D., 2011. Structure
356 and reactivity of the calcite–water interface. J. Coll. Inter. Sci. 354, 843-857.
357 Inguaggiato, C., Censi, P., Zuddas, P., D'Alessandro, W., Brusca, L., Pecoraino, G., Bellomo, S.,
358 2016. Zirconium-hafnium and rare earth element signatures discriminating the effect of
359 atmospheric fallout from hydrothermal input in volcanic lake water. Chem. Geol. 433, 1–11.

Inguaggiato, C., Censi, P., Zuddas, P., Londono, J.M., Chacon, Z., Alzate, D., Brusca, L., D'Alessandro, W., 2015. Geochemistry of REE, Zr and Hf in a wide range of pH and water composition: the Nevado del Ruiz volcano-hydrothermal system (Colombia). Chem. Geol. 417, 125–133.

Jakubowicz, M., Dopieralska, J., Belka, Z., 2015. Tracing the composition and origin of fluids at an ancient hydrocarbon seep (Hollard Mound, Middle Devonian, Morocco): A Nd, REE and stable isotope study. Geochim. Cosmochim. Acta 156, 50-74.

Jochum, K.P., Seufert, H.M., Spettel, B., Palme, H., 1986. The solar-system abundances of Nb, Ta, and Y, and the relative abundances of refractory lithophile elements in differentiated planetary bodies. Geochim. Cosmochim. Acta 50, 1173-1183.

Johannesson, K.H., Lyons, W.B., 1994. The rare earth element geochemistry of Mono Lake water and the importance of carbonate complexing. Limnology and Oceanography 39 (5), pp. 1141-1154.

Johannesson, K.H., Lyons, W.B., Bird, D.A., 1994. Rare earth element concentrations and speciation in alkaline lakes from the western U.S.A. Geophysical Research Letters 21, 773-776.

Jones, J.V., III, Piatak, N.M., and Bedinger, G.M., 2017, Zirconium and hafnium, chap. V of Schulz, K.J., DeYoung, J.H., Jr., Seal, R.R., II, and Bradley, D.C., eds., Critical mineral resources of the United States—Economic and environmental geology and prospects for future supply: U.S. Geological Survey Professional Paper 1802, p. V1– V26, https://doi.org/10.3133/pp1802V.

Kagi, H., Dohmoto, Y., Takano, S. and Masuda, A., 1993. Tetrad effect in lanthanide partitioning between calcium sulphate crystal and its saturated solution. Chem. Geol. 107, 71-82.

Kerrich, R., Renaut, R.W., Bonli, T., 2002. Trace-element composition of cherts from alkaline lakes in the east African rift: a probe for ancient counterparts. Spec. Publ. 73, 277–298.

Koschinsky, A., Hein, J.R., 2003. Uptake of elements from seawater by ferromanganese crusts: Solid-phase associations and seawater speciation. Mar. Geol. 198, 331-351.

Lee J.H., Byrne R. H. (1993). Complexation of trivalent rare earth elements (Ce, Eu, Gd, Tb, Yb) by carbonate ions. Geochim. Cosmochim. Acta 57, 295–302.

Lemaitre, N., Bayon, G., Ondréas, H., Caprais, J.C., Freslon, N., Bollinger, C., Rouget M.-L., De Prunelé A., Ruffine L., Olu-Le Roy K., Sarthou G., 2014. Trace element behaviour at cold seeps and the potential export of dissolved iron to the ocean. Earth Planet. Sci. Lett. 404, 376-388.

Lin, J., Nilges, M.J., Wiens, E., Chen, N., Wang, S., Pan, Y., 2018. Mechanism of Gd^{3+} uptake in gypsum ($CaSO_4 \cdot 2H_2O$): Implications for EPR dating, REE recovery and REE behavior. Geochim. Cosmochim. Acta 258, 63-78.

Liu, X.W., Byrne, R.H., 1998. Comprehensive investigation of yttrium and rare earth element complexation by carbonate ions using ICP-mass spectrometry. J. Solution Chem. 27, 803-815.

Michard A.,1989. Rare earth systematics in hydrothermal fluids. Geochim. Cosmochim. Acta 53, 745–750.

Michard A., Albarede F., 1986. The REE contents of some hydrothermal fluds. Chem. Geol. 55, 51–60.

Moller, P., Bau, M. 1993. Rare-earth patterns with positive cerium anomaly in alkaline waters from Lake Van, Turkey. Earth Planet. Sci Lett. 117, 671-676.

Möller, P., De Lucia, M., 2020. Incorporation of rare earths and yttrium in calcite: A critical re-evaluation. Aquat. Geochem., 26 (2020), pp. 89-117

Parisi, M. G., Cammarata, I., Cammarata, M., Censi, V., 2017. Rare earths, zirconium and hafnium distribution in coastal areas: The example of Sabella spallanzanii (Gmelin, 1791). Chemosphere 185, 268-276.

Parkhurst, D.L., Appelo, C.A.J., 2010. User's Guide to PHREEQC (Version 2.17.5) - A Computer program for Speciation, Batch- Reaction, One-Dimensional Transport and Inverse Geochemical Calculations. Available at: http://www.brr.cr.usgs.gov/projects/ GWC_coupled/phreeqc/index.html.)

410 Phan, T.T., Hakala, J.A., Lopano, C.L., Sharma S., 2019. Rare earth elements and radiogenic
411 strontium isotopes in carbonate minerals reveal diagenetic influence in shales and limestones in
412 the Appalachian Basin. Chem. Geol. 509, 194-212.
413 Pinto, H., Haapasilta, V., Lokhandwala, M., Oberg, S., Foster, A.S., 2017. Adsorption and migration
414 of single metal atoms on the calcite (10.4) surface. J. Phys.-Condes. Mat. 29, (13)
415 Playà, E., Cendon, D.I., Trave, A., Chivas, A.R., Garcia, A., 2007. Non-marine evaporites with both
416 inherited marine and continental signatures: The Gulf of Carpentaria, Australia, at similar to 70
417 ka. Sed. Geol 201, 267-285.
418 Qu, C.L., Liu, G., Zhao, Y.F., 2009. Experimental study on the fractionation of yttrium from
419 holmium during the coprecipitation with calcium carbonates in seawater solutions. Geochem. J.
420 43, 403-414.
421 Raso, M., Censi, P., Saiano, F., 2013. Simultaneous determinations of zirconium, hafnium, yttrium
422 and lanthanides in seawater according to a co-precipitation technique onto iron-hydroxide.
423 Talanta 116, 1085–1090.
424 Reynard, B., Lécuyer, C., Grandjean, P., 1999. Crystal-chemical controls on rare-earth element
425 concentrations in fossil biogenic apatites and implications for paleoenvironmental
426 reconstructions. Chem. Geol. 155, 233-241.
427 Scarlett N.V.Y., Madsen I.C., 2006. Quantification of phases with partial or no known crystal
428 structures. Powder Diffraction 21, 278-284.
429 Sillen, L.G., Martell, A.E., 1964. Stability Constants of Metal–Ion Complexes, Special Publication
430 17, The Chemical Society, London, pp 754.
431 Taylor, S.R., McLennan, S.M., 1988. The significance of the rare earths in geochemistry and
432 cosmochemistry. Handbook on the Physics and Chemistry of Rare Earths, cap. 79, vol. 11, 485-
433 578.
434 Taylor, S.R., McLennan, S.M., 1995. The geochemical evolution of the continental crust. Rev.
435 Geophys. 33, 241–265.

436 Tepe, N., Bau, M., 2015. Distribution of rare earth elements and other high field strength elements in
437 glacial meltwaters and sediments from the western Greenland Ice Sheet: evidence for different
438 sources of particles and nanoparticles. Chem. Geol. 412, 59–68.
439 Thompson, A., Amistadi, M.K., Chadwick, O.A., Chorover, J., 2013, Fractionation of yttrium and
440 holmium during basaltic soil weathering. Geochem. Cosmochim. Acta 119, 18-30.
441 Toulkeridis, T., Podwojewski, P., Clauer, N., 1998. Tracing the source of gypsum in New
442 Caledonian soils by REE contents and S-Sr isotopic compositions. Chem. Geol. 145, 61-71.
443 Tripathy, S.S., Kanungo, S.B., Mishra, S.K., 2001. The electrical double layer at hydrous manganese
444 dioxide/electrolyte interface. J. Colloid Interface Sci. 241, 112–119.
445 Wang, J.; Chang, J.; Li, C.; Han, Z.; Wang, T.; Han, H., 2020. Significance of Calcite Trace
446 Elements Contents and C-O Isotopic Compositions for Ore-Forming Fluids and Gold Prospecting
447 in the Zhesang Carlin-Like Gold Deposit of Southeastern Yunnan, China. Minerals 10, 338.
448 Yilmaz, Y., 1990. Comparison of young volcanic associations of western and eastern Anatolia
449 formed under a compressional regime: a review. Jour. Volcan. Geoth. Res. 44, 69-87.
450 Young, R. The Rietveld Method, International Union of Crystallography, Oxford University Press,
451 Oxford, 1993.
452 Zhang, L., Algeo, T.J., Cao, L., Zhao, L., Chen, Z.-Q., Li, Z., 2016. Diagenetic uptake of rare earth
453 elements by conodont apatite. Palaeogeogr. Palaeoclimatol. Palaeoecol. 458, 176–197.
454 Zuddas, P., Censi, P., Inguaggiato, C., Sposito, F., 2018 The behaviour of zirconium and hafnium
455 during water-rock interaction. Appl. Geochem. 94, 46–52.
456 Zuddas, P., Inguaggiato, C., Censi, P., D'Alessandro, W., 2017. Zr-Hf fractionation during water-
457 rock interaction. Procedia Earth and Planetary Science 17, 670-673.
458

TABLE CAPTIONS

Table 1 - Sampling sites and geographical localisation of studied waters.

Table 2 - Mineralogical composition of studied suspended particulates in lake waters. Values are given in weight %.

FIGURE CAPTIONS

Figure 1 – Geological sketch map of the studied area.

Figure 2 – Major element concentrations analysed in studied waters.

Figure 3 – SEM images of suspended solids in studied water samples filtered with membrane porosity 0.45 µm. Fig. 3a, 3b, 3c, and 3d: Different amounts of build-up in suspended solids mixed to authigenic carbonates in lake waters from different sites. Fig. 3e and 3f: Some particulars of well-developed calcite crystals together with biologic remnants in lake waters. Fig. 3g and 3h: Authigenic solids and lithic fragments are suspended in thermal springs. Fig. 3i: Fine-grained Ca-Mg carbonates and Fe-bearing solids in suspended particles from thermal springs. The open square indicates the area where data to depict X-ray Fluorescence maps of Fe, Ca, and Mg were collected.

Figure 4 – a: Zr and Hf concentration measured in studied water samples and the linear trend depicted by these analyses. b: Zr and Hf concentration measured in suspended solids in studied water samples. c: Zr and Hf concentration measured in halite crystallising from the Dead Sea brine (data from Censi et al., 2020). Measured Zr and Hf concentrations are compared with the range of Zr/Hf values characteristic of crustal rocks and chondrite (Zr/Hf = 71 ± 6, Jochum et al., 1986).

Figure 5– Zr/Hf values measured in the dissolved phase of the lake and thermal waters reported towards Ca^{2+} concentration (mol/L) expressed as pCa (see equation 4).

Figure 6 – Shale-normalised REE pattern calculated in the dissolved phase of the lake (a) and thermal waters (b). These features are also depicted in terms of MREE/HREE and LREE/MREE ratios (c). Shale-normalised REE pattern calculated for suspended solids in the lake (d) and thermal waters (e). These features are also reported in terms of MREE/HREE and LREE/MREE ratios (f).